nature reviews materials

https://doi.org/10.1038/s41578-023-00587-5

Review article

Check for updates

3D-printed PEDOT:PSS for soft robotics

Jinhao Li [1,2,4], Jie Cao [3,4], Baoyang Lu [3] ✉ & Guoying Gu [1,2] ✉

Abstract

Soft robotics is an emerging technology requiring conductive materials with inherently high compliance to sense, control or actuate. Poly(3,4-ethylenedioxythiophene):polystyrene sulfonate (PEDOT:PSS) is a soft and flexible conducting polymer with tunable mechanical properties, mixed ionic and electronic conductivity and excellent processability. Combining PEDOT:PSS with advanced 3D printing has ushered unprecedented opportunities in soft material engineering and soft robotics. In this Review, we aim to bridge the gap between different research areas by specifically discussing the use of PEDOT:PSS-based inks in 3D printing for soft robotics. We discuss rational PEDOT:PSS-based ink design and evaluation, 3D-printing technologies and strategies as well as applications for soft robotics. We provide insights into the theoretical background and fundamental aspects of the 3D printing of conducting polymers, with the goal of accelerating soft robotics development.

Sections

[1]Robotics Institute and State Key Laboratory of Mechanical System and Vibration, School of Mechanical Engineering, Shanghai Jiao Tong University, Shanghai, China. [2]Meta Robotics Institute, Shanghai Jiao Tong University, Shanghai, China. [3]Jiangxi Key Laboratory of Flexible Electronics, Flexible Electronics Innovation Institute, Jiangxi Science and Technology Normal University, Nanchang, China. [4]These authors contributed equally: Jinhao Li, Jie Cao. ✉e-mail: luby@jxstnu.edu.cn; guguoying@sjtu.edu.cn

Introduction

By merging biological concepts and robotic systems, soft robotics has emerged as a technology with applications across length scales, from micrometre-scale clinical medicine (such as in drug delivery[1,2] or neurovascular interventions[3,4]), millimetre-scale consumer electronics (such as in precise manipulation[5,6] or tactile feedback[7–9]) to metre-scale motion enhancement (such as in exoskeletons[10] or during rehabilitation assistance[11]). Contrary to traditional rigid robots, the materials used in soft robots are characterized by their low Young's modulus (typically <1 GPa), providing inherent compliance and adaptiveness in unstructured environments[12]. Soft materials for robotic systems can be roughly categorized into passive materials (such as silicone or textiles) acting as adaptable frameworks and active materials (such as dielectric elastomers and liquid crystal elastomers) with stimuli-response and embodied intelligence[13,14]. In addition, compliant conductive materials are essential to fabrication of soft robots, but there is a substantial mismatch among the design, fabrication and integration of rigid conductors, such as metals, into soft robots. For example, improving stretchability using structure engineering compromises device density and ease of processing[15,16]. Stacking thin-film devices as an assembly strategy commonly introduces mechanical mismatch, thus limiting robustness and versatility for locomotion and manipulation in applications[17,18]. Alternatively, soft conductors, such as conducting polymers, liquid metals, ionic hydrogels and conductive filler and/or elastomer composites[19–23], provide a straightforward and reliable route for systematic integration. Among those, the conducting polymer poly(3,4-ethylenedioxythiophene):polystyrene sulfonate (PEDOT:PSS) is one of the most promising candidates because of its soft and flexible mechanical properties, mixed ionic and electronic conductivity, aqueous dispersibility and biocompatibility[24–28] and creating unprecedented opportunities towards merging humans and robots[29–31].

One of the grand limitations of PEDOT:PSS-based soft robotics stems from fabrication. Although digital-customized cross-scale manufacturing for 3D architectures remains the objective, existing machines and robots usually rely on 2D fabrication techniques such as casting[32], printing[33,34] or lithography[35,36] to produce thin-film patterns. These methods have complicated procedures and can be wasteful owing to subtractive manufacturing. Methods such as moulding have been frequently used to fabricate 3D entities but are high cost and provide low resolution (>100 μm)[37]. Benefiting from the cross-scale customizability enabled by computer control, 3D-printing technologies are capable of mass personalization and rapid prototyping with high resolution[38,39]. Wide material compatibility and one-step assembly also allow task-specific material design and integration for diverse soft robotic applications.

The convergence among conducting polymers, 3D printing and soft robotics is explosively growing, with demonstrated integrations in complex systems such as soft bioelectronics, sensors and actuators[40–46]. Several reviews already cover individual topics such as conducting polymers[47], 3D-printing techniques[48] and soft robotics[49]. Some reviews have combined pairwise overlapping fields to accelerate the designs for specific tasks, including 3D-printable functional inks[38,50], conductive hydrogels suitable for soft robotics[51–53] and 3D-printed soft robotic systems[54–56]. However, these reviews do not account specifically for the 3D printing of conducting polymers for soft robotics. Such a systematic discussion is essential for the future development of this emerging and impactful field.

In this Review (Fig. 1), we start by overviewing rational 3D-printable PEDOT:PSS-based ink design methodologies across multiple scales and their underlying mechanisms. Then, we present guidelines to evaluate ink printability, enabling the comparison and further improvement of various ink systems. We summarize the evolution and latest advances in 3D-printing techniques for conducting polymers, providing critical commentary on fabrication strategies to enable further integration. Finally, we discuss ongoing applications for soft robotics and provide insights into future opportunities and challenges, such as high-performance inks, advanced printing technologies and robust integration towards soft robotic systems.

PEDOT:PSS-based precursor inks

As a dimension-raising manufacturing technology, 3D printing can be categorized as either nozzle-based or light-based printing. PEDOT:PSS-based precursor inks need to be rationally designed to fulfil the requirements of 3D-printed architectures (Box 1). Typical design strategies include molecular engineering (such as molecular structural design and chain–chain interaction), phase engineering (multilength scales ranging from nanometres to micrometres or even millimetres) and morphology modulation. These strategies use multiple molecular and phase interactions to redesign components and have been successfully implemented in several printable PEDOT:PSS-based ink systems, including pure PEDOT:PSS and PEDOT:PSS composited with secondary dopants, viscoelastic polymers, conductive fillers and photopolymers (Table 1). To enable printable PEDOT:PSS dispersions, rational ink design based on the optimization of the rheological properties and the composition of the ink is essential. In this section, we briefly summarize varying 3D-printable PEDOT:PSS-based inks (Fig. 2), and we discuss the corresponding design principles and their underlying mechanisms.

Pure PEDOT:PSS inks

Pure PEDOT:PSS inks are prepared by directly treating commercial PEDOT:PSS dispersions without introducing any extra components. Several approaches have been developed to optimize the viscosity of the solution for 3D printing.

The most straightforward method is directly condensing the commercial PEDOT:PSS solution to improve its solid content. For example, upon vigorous stirring at 120 °C for 3 h (ref. 57), around two-thirds of the water in pristine PEDOT:PSS aqueous solution can be evaporated, leading to the formation of viscoelastic inks (~2×10^4) with an improved solid content of ~3 wt% PEDOT:PSS. The resultant pure PEDOT:PSS ink is processable by nozzle-based 3D printing, although it requires external assistance through, for example, post-printing crosslinking[43,57,58], to maintain its printed shape. However, such a heating and condensing process is time-consuming and generally results in irreversible and unmanageable aggregation of π-conjugated PEDOT chains, which inevitably induces substantial inhomogeneities in the resultant PEDOT:PSS ink. Because PEDOT:PSS clusters and/or aggregates affect the fluency, continuity and resolution of the printing process, further processing techniques such as filtration and homogenization are required to remove them after condensation[59].

An alternative approach to prepare 3D-printable pure PEDOT:PSS inks is to lyophilize commercial PEDOT:PSS aqueous solutions to afford dry re-dispersible PEDOT:PSS pellets, which is more controllable and scalable[46,60]. The detailed procedure involves rapidly freezing and successively drying a commercial PEDOT:PSS dispersion in extremely low-temperature environments such as liquid nitrogen[60], followed by the re-dispersion of the dried PEDOT:PSS pellets in water or water-based multisolvent systems. The irreversible formation

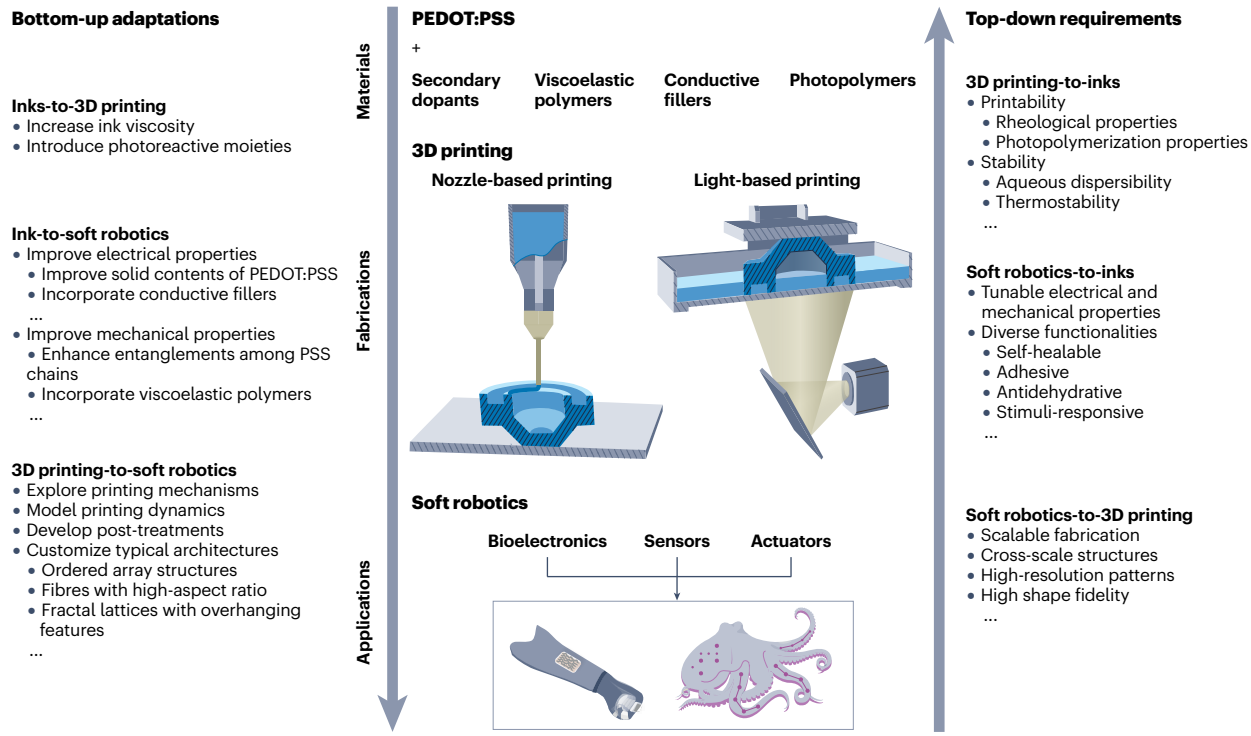

Fig. 1 | Roadmap on 3D-printing poly(3,4-ethylenedioxythiophene):polystyrene sulfonate for soft robotics. Printable poly(3,4-ethylenedioxythiophene):polystyrene sulfonate (PEDOT:PSS)-based ink systems, including pure PEDOT:PSS and PEDOT:PSS composites, enable soft robotic systems by either nozzle-based or light-based printing. In this methodology, great efforts have been devoted to bridging materials, fabrications and applications, considering bottom-up adaptations and top-down requirements.

and aggregation of PEDOT-rich crystalline domains through π–π stacking can be effectively prevented owing to accelerated ice crystal formation during the lyophilization in a cryogenic condition. Redispersion of the obtained PEDOT:PSS pellets in water facilitates the preparation of 3D-printable inks with more controllable weight ratios and viscosity, which adequately fulfils the demands of nozzle-based 3D printing.

PEDOT:PSS-secondary dopant inks

Secondary dopants are generally 'inert' substances that can further modify the performance of primary-doped polymers, relying on phase separation and polymer chain re-arrangement[61]. The most commonly used secondary dopants for PEDOT:PSS are mainly high boiling point strong polar solvents such as dimethyl sulfoxide (DMSO)[46,62,63] and ethylene glycol[64,65], strong acids such as concentrated sulfuric acid[28] and ionic liquids[66]. Theoretically, dopants with strong polarity or even ionic species can exert charge screening, which weakens the Coulombic interaction between $PEDOT^+$ and PSS^-. This weakened Coulombic interaction can result in the partial aggregation of PEDOT forming PEDOT-rich domains with higher crystallinity[67]. Macroscopically, these changes give rise to important phase separation between PEDOT and PSS, reflected as viscosity increments and even weak physical gelation resulting from multiple intermolecular interactions. All these chain conformational changes as well as the correspondent rheological evolution promote the transformation of dilute PEDOT:PSS dispersions to viscous 3D-printable inks.

Using these fundamental understandings, 3D-printable PEDOT:PSS inks were developed by directly adding DMSO into commercial PEDOT:PSS dispersions to realize the successful 3D printing of a complex wavy-meshed pattern with a resolution of 400 μm (ref. 68). In addition, by mixing lyophilized PEDOT:PSS pellets with water–DMSO binary solvent at the optimal concentration of 5–7 wt%, PEDOT:PSS inks that had the desired shear-thinning and shear-yielding properties for 3D printing were easily prepared. These inks had excellent stability without obvious degradation of their rheological properties or modification of their printability after 6-week storage in ambient conditions[46].

Alternatively, using 4-dodecylbenzenesulfonic acid (DBSA) as the secondary dopant led to 3D-injectable PEDOT:PSS-DBSA inks with controllable gelation time[28]. By providing adequate H^+ to protonate PSS^-, DBSA markedly weakens the electrostatic force between PEDOT and PSS, leading to a connected physical network with increased viscosity, which is useful for continuous extrusion. Other effective secondary dopants such as concentrated sulfuric acid[69] and ionic liquids[66] simultaneously improve the viscosity and electrical conductivity of PEDOT:PSS, potentially enabling the realization of 3D-printable inks.

PEDOT:PSS-viscoelastic polymer inks

Viscoelastic polymers combine both the advantages of viscous liquids and elastic solids[70]. The incorporation of such viscoelastic polymers into PEDOT:PSS is an effective methodology to simultaneously endow PEDOT:PSS-based inks with excellent 3D printability and to improve the mechanical performance of the printed patterns[71]. Typical hydrophilic

viscoelastic polymers such as polyacrylamide, poly(acrylic acid), poly(vinyl alcohol) (PVA)[44,72,73], poly(ethylene oxide) (PEO)[42,74,75], carboxyl methyl cellulose[76] and polyurethane (PU)[45] have been composited with PEDOT:PSS to prepare stable 3D-printable inks.

Currently, 3D-printable PEDOT:PSS-viscoelastic polymer inks are mainly prepared by direct mechanical blending, that is, by mixing viscoelastic polymer aqueous solution and PEDOT:PSS dispersion or dried pellets using vigorous mechanical agitation[44,74]. During such a process, enhanced entanglement among PSS and/or long polymer chains, together with friction among polymer chains, lead to a substantial viscosity increase. By regulating the concentration of both components (namely, the density of polymer networks), the viscosity of the resultant inks can be controlled over a wide range of 1–10^5 Pa s. Notably, hydrophilic viscoelastic polymers that have functional groups such as -OH, -SO_3H or -COOH can break the Coulombic force between $PEDOT^+$ and PSS^- chains and facilitate the conformational rearrangement of PEDOT, while simultaneously acting as effective secondary dopants. For example, the vigorous mechanical blending of redispersed PEDOT:PSS pellets and a PVA viscous solution resulted in an homogeneous 3D-printable PEDOT:PSS-PVA ink[44]. Such an ink demonstrated both shear-thinning and shear-yielding properties, enabling excellent extrusion and shape fidelity for nozzle-based 3D printing. On post-treatment such as freeze–thawing, structures made using PEDOT:PSS-PVA inks had improved mechanical properties compared with the weak and brittle structures made of pure PEDOT:PSS, because of hydrogen bonding-crosslinked PVA chains.

Although the introduction of viscoelastic polymers into PEDOT:PSS inks can effectively enhance the mechanical performance of 3D-printed architectures, one critical challenge is the inevitable compromise of the electrical properties of resultant materials, which limits their utilization for soft robotics that simultaneously requires excellent mechanical and electrical performance. To overcome this obstacle, an innovative bi-continuous ink design strategy has been proposed by compositing hydrophilic polymers such as water-borne PU (not water-soluble but swellable) with PEDOT:PSS, well addressing the trade-off between electrical and mechanical properties[77]. PEDOT:PSS is used as an electrical phase, whereas hydrophilic PU acts as a mechanical phase. Owing to the different solubility of PEDOT:PSS and PU in water and ethanol, PEDOT:PSS forms aggregates in the ethanol–water solvent system when the ethanol concentration reaches >70 vol.%, whereas hydrophilic PU shows phase separation when the ethanol concentration is <70 vol.%. Interestingly, both PEDOT:PSS and hydrophilic PU are slightly phase-separated but free of substantial aggregation in 70 vol.% ethanol–30 vol.% water, generating homogeneous 3D-printable inks with pre-formed phase-separated PEDOT:PSS phases with good electrical conductivity and PU phases with good mechanical properties[45]. Starting from the optimal ink composition, evaporating the solvent and successively equilibrating in aqueous solution after printing led to a bi-continuous conducting polymer hydrogel of PEDOT:PSS and PU with simultaneously high electrical conductivity (>10 S cm^{-1}), stretchability (>300% strain) and fracture toughness (3,000 J m^{-2}).

PEDOT:PSS-conductive filler inks

Although PEDOT:PSS films exhibit relatively high electrical conductivity (over 10^3 S cm^{-1}), such performance is still vastly inferior to typical electronic conductors such as metals[24,78], carbon nanotubes[79] or graphene[80]. A further enhancement of the electrical properties of PEDOT:PSS-based inks (such as higher electrical conductivity, lower interfacial impedance, higher charge storage capacitance and higher injection capacity) is expected to lead to more opportunities for robotic applications such as soft wiring[81,82].

The preferred route to improve the electrical properties of PEDOT:PSS is to incorporate highly conductive fillers. Interestingly, these conductive fillers are also effective additives to optimize the rheological properties of pristine PEDOT:PSS inks owing to diverse induced interactions with PEDOT:PSS segments[59]. A wide range of

Box 1

The fundamentals of poly(3,4-ethylenedioxythiophene):polystyrene sulfonate

Poly(3,4-ethylenedioxythiophene):polystyrene sulfonate (PEDOT:PSS), first synthesized in the late 1980s[212], is a water-soluble macromolecular dispersion with tunable solid contents (1.0–3.0 wt%) of hydrophobic PEDOT and hydrophilic PSS[213]. The polyelectrolyte PSS is a charge-balancing counterion and can drastically promote the dispersion of PEDOT in water, thus enabling its excellent solution processability. In aqueous dispersions, PEDOT:PSS tends to form colloidal microparticles with a core–shell structure in which an excess of PSS-rich shell encapsulates the PEDOT-rich core (the weight ratios of PEDOT to PSS range from 1:2.5 to 1:25)[214].

The molecular interactions in PEDOT:PSS are mainly electrostatic forces between the conducting conjugated PEDOT and insulating PSS, π–π stacking among adjacent PEDOT chains and entanglement among long PSS chains[68]. Considerable works have been dedicated to the modification of these molecular interactions to design PEDOT:PSS with improved electrical and/or mechanical properties for diverse applications. Commercial PEDOT:PSS products, including Clevios PH500, PH1000, Orgacon S315, DRY and so on, have been attracting lots of attention owing to their tunable electrical conductivity and favourable aqueous dispersibility, which continue to grow in markets with an estimated annual value of over $50 billion[59].

Currently, PEDOT:PSS patterns, structures and devices are generally fabricated by casting, printing and lithography, limiting the customizability, integration and fabrication of 3D structures. The inherent characteristics of pristine PEDOT:PSS aqueous dispersions, such as their low solid content (1.0–3.0 wt%), high water content (90–95%) and low viscosity (<0.1 Pa s), are associated with immense challenges for the development of dimension-raising fabrication techniques such as nozzle-based and light-based 3D printing.

Table 1 | Typical 3D-printed poly(3,4-ethylenedioxythiophene):polystyrene sulfonate-based polymers: properties, fabrication and performances

Categories	Ink components	Printing technique	Resolution (μm)	Crosslinking method	Mechanical properties of hydrogels	Conductivity of dry films (S cm^{-1})	Ref.
Pure PEDOT:PSS inks	PEDOT:PSS	DIW	20	Ionic crosslinking	*E* = ~30.7 kPa	600	58
	PEDOT:PSS	DIW	118	Annealing	NA	15.7	123
PEDOT:PSS-secondary dopants inks	PEDOT:PSS-DMSO	MGP	0.135	Drying	δ = 270%	0.01–200	108
	PEDOT:PSS-DMSO	IJP	44	Drying	δ = 40%	NA	122
	PEDOT:PSS-DMSO	DIW	30	Annealing	*E* = ~1.1 MPa	155	46
	PEDOT:PSS-EG	DIW	0.7	Drying	*E* = 150 MPa (fibre)	70	65
	PEDOT:PSS-DBSA	DIW	200	NA	δ = 300%	0.1	28
	PEDOT:PSS-ethanol	MGP	0.6	Drying	NA	NA	109
PEDOT:PSS-viscoelastic polymer inks	PEDOT:PSS-PEO	IJP	~27.25	Drying	NA	NA	76
	PEDOT:PSS-PVA	DIW	500	Freeze–thawing	δ = ~300%	NA	44
	PEDOT:PSS-MC-κCA	DIW	NA	Ionic-crosslinking	NA	~0.003[a]	150
	PEDOT:PSS-CMC	DIW	200	Drying	NA	10.3	77
	PEDOT:PSS-PU	DIW	NA	Drying	δ = ~400%	11[a]	45
	PEDOT:PSS-GelMA	DIW	120	Light-crosslinking	*E* = 40–150 kPa	NA	125
PEDOT:PSS-conductive filler inks	PEDOT:PSS-Ag	DIW	38	Drying	NA	NA	79
	PEDOT:PSS-CNTs	DIW	200	Drying	δ = 150%[b]	NA	80
	PEDOT:PSS-MXene	DIW	NA	Ionic-crosslinking	δ = ~7.7%	55.17[a]	86
	PEDOT:PSS-MXene	DIW	250	Drying	NA	100–1,600	87
	PEDOT:PSS-MoS_2	DIW	NA	Drying	NA	49.01	88
PEDOT:PSS-photopolymer inks	PEDOT:PSS-PEGDA	TPP	1	Photopolymerization	NA	281	102
	PEDOT:PSS-PEGDA	SLA	NA	Photopolymerization	NA	0.055	135
	PEDOT:PSS-AAm-PEGDA	DLP	70	Photopolymerization	*E* = 12.3–18.2 kPa	0.017[a]	101

δ, maximum tensile strain; AAm, acrylamide; CMC, carbon methyl cellulose; CNT, carbon nanotube; DBSA, 4-dodecylbenzenesulfonic acid; DIW, direct ink writing; DLP, digital light processing; DMSO, dimethyl sulfoxide; *E*, Young's modulus; EG, ethylene glycol; GelMA, gelatin methacryloyl; IJP, inkjet printing; MC-κCA, methylcellulose and κ-carrageenan; MGP, meniscus-guided printing; NA, not applicable; PEDOT:PSS, poly(3,4-ethylenedioxythiophene):polystyrene sulfonate; PEGDA, poly(ethylene glycol) diacrylate; PEO, poly(ethylene oxide); PU, polyurethane; PVA, poly(vinyl alcohol); SLA, stereolithography; TPP, two-photon polymerization. [a]Conductivity of hydrogels. [b]Mechanical properties of dry films.

highly conductive nanomaterials such as nano-structured metals, carbon nanotubes, nanowires or nanoribbons, graphene and other 2D-materials[83,84], including MXenes[85,86] and MoS_2 (ref. 87), have been composited with the PEDOT:PSS matrix to simultaneously modify its electrical and rheological properties.

In such a composite system, the conductive fillers enable the formation of printable inks for nozzle-based 3D printing, and the PEDOT:PSS dispersion acts as both the binder and the support skeleton to bridge the conductive fillers[83]. Controllable rheological properties can be easily achieved through the tuning of the PEDOT:PSS to conductive filler ratio. With an increment in the concentration of conductive fillers, the suspensions can progressively be converted from low-viscosity liquids to physical gels with viscoelastic performances (10^2–10^5 Pa s) that are appropriate for extrusion printing[83]. Owing to the presence of electrostatic forces or π–π stacking in the reversible physical network, conductive fillers can uniformly disperse in PEDOT:PSS dispersions and further facilitate the formation of a continuous conductive phase. In addition, conductive fillers substantially enhance the ink viscosity and maintain the balance between mechanical and electrical performances. Inspired by the characteristic physical gels, many studies adopt this strategy to prepare viscous inks with the pre-crosslinking network for satisfying the requirement of 3D printing[88]. Furthermore, conductive fillers are tightly arranged along the extrusion orientation in the printing process, which considerably improves the properties of printed structures such as electrical, thermoelectric and mechanical performance. However, the inclusion of excessive amounts of conductive fillers leads to agglomeration among the PEDOT:PSS network[59], which results in inhomogeneous inks and poor connection at the joints between the fillers and PEDOT:PSS. This inhomogeneity seriously impedes both the extrusion through nozzles and the formation of conducting pathways in the printed structures.

PEDOT:PSS-photopolymer inks

A pivotal condition in preparing PEDOT:PSS-based inks for light-based printing is to introduce photoreactive moieties such as reactive alkenes, acrylates and methacrylates for free-radical polymerization. Photopolymers act as carriers for photoreactive moieties and typically include acrylamide, poly(ethylene glycol) (PEG), PEG diacrylate (PEGDA) and PEG dimethacrylate (PEGDMA)[89,90]. Additionally, viscosity modifiers (such as poly(*N*-vinylpyrrolidone) or DMSO) are also added

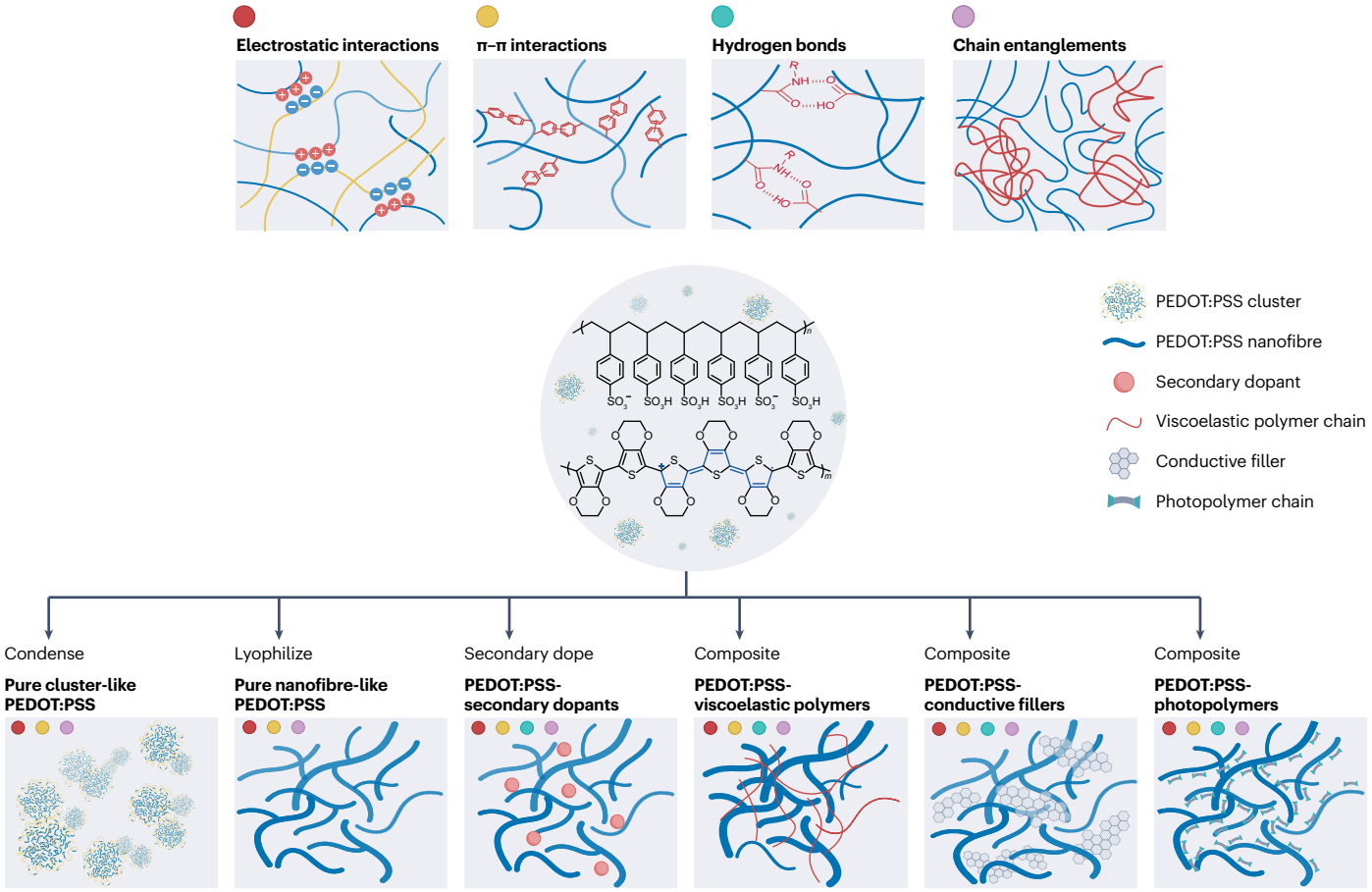

Fig. 2 | Design strategies and schematic illustrations for 3D-printable poly(3,4-ethylenedioxythiophene):polystyrene sulfonate-based inks. Internal non-covalent interactions (such as electrostatic interactions, π–π interactions, hydrogen bonds and chain entanglements) are marked as coloured dots. PEDOT:PSS, poly(3,4-ethylenedioxythiophene):polystyrene sulfonate. Partly adapted with permission from ref. 13. Copyright 2021 American Chemical Society.

to PEDOT:PSS-photopolymer inks to regulate their viscosity, ensuring appropriate flowability during the printing process[43]. For example, in a double network containing PEDOT:PSS and PEGDMA, the photoinitiator Irgacure 2959 (which absorbs light irradiation to generate radicals) triggered PEGDMA chain growth to form an interpenetrating covalent crosslinked network[36].

Three-dimensional-printing techniques

Three-dimensional printing is a low-cost and scalable fabrication technology that patterns and crosslinks bulky PEDOT:PSS-based inks layer by layer[38,48] (Fig. 3a,b) and enables the fabrication of customized cross-scale structures. The printed architectures generally scale up from submicron scale to submetre scale (Fig. 3c), covering the needs of soft robotic systems.

Three-dimensional printing can be categorized as either nozzle-based or light-based printing. Nozzle-based printing uses nozzle-based printheads to shape precursor inks into desired architectures in serial. Then, the printed fluids are transited to solids and/or gels by post-treatment. During the printing process, precursor inks with varying rheological properties exhibit different shear-thinning behaviours and resultant fluid morphologies. Depending on the desired fluid morphology, typical nozzle-based printing techniques include meniscus-guided printing (MGP) (meniscus), inkjet printing (IJP) (droplets) and direct ink writing (DIW) (filaments) (Fig. 3a). Alternatively, light-based printing offers high resolution and rapid fabrication for photosensitive polymers. This technique simultaneously patterns and crosslinks precursor inks by light irradiation, ensuring high shape fidelity[54]. Depending on the irradiation source, typical light-based printing techniques include stereolithography (SLA) (laser facula), two-photon polymerization (TPP) (two-photon) and digital light processing (DLP) (light projection) (Fig. 3a).

Evaluation guidelines for ink printability

The evaluation of the printability of the ink facilitates rapid iterations of the composition of the ink and the optimization of the printing mechanism. A comprehensive protocol is indispensable to characterize, evaluate and compare diverse ink components, but such a protocol is lacking for PEDOT:PSS-based inks. Herein, we summarize the desired rheological and photopolymerization properties contributing to 3D-printable inks and then use them as guidelines to compare fabricating strategies.

Rheological properties for nozzle-based printing. Rheological properties describe the deformation or flow of precursor inks in response to applied shear force or stress. Precursor inks that have moderate rheological properties avoid uncontrollable spreading or clogging nozzle-based printheads (Fig. 3d).

Specifically, inks with shear-thinning properties have decreased viscosities under an increasing shear rate, enabling them to be shaped in different morphologies. To facilitate the comparison, we recommend reporting the viscosity at characteristic shear rates, corresponding to different nozzle-based printing techniques, as the apparent viscosity. The typical apparent viscosities of printable inks are summarized in Fig. 3e. Low-viscosity PEDOT:PSS inks (<0.1 Pa s) commonly have weak shear-thinning properties. The surface tension for IJP printable fluids[91,92] can also be used for printability evaluation, using, for example, the Ohnesorge number – a dimensionless number comparing viscous forces with inertial and surface tension forces (Fig. 3f). Specifically, the surface tension affects the uniformity of jetted films. Typical surface tensions for PEDOT:PSS-based printable inks range from 25 mN m^{-1} to 80 mN m^{-1}, which prevents the edge line recession of droplets or coffee-ring effects[93,94]. Surface tension gradients in the MGP process induce Marangoni flow (liquid–gas interfacial motions caused by locally differentiated composition or temperature) towards the printing nozzle or enhance the flow to the solid–liquid contact line as solutal Marangoni flow[95,96].

Another important factor is the shear-yielding properties, which theoretically describe the barrier on shear-induced gel–sol transition (typically, shear yield stress). Generally, shear yield stress uses the shear stress at the crossover of storage modulus and loss modulus ($\tau_y = \{\tau: G' = G''\}$)[97], indicating the transition from solid-like ($G' > G''$) to liquid-like ($G' < G''$) behaviour (Fig. 3g). Sufficient shear yield stress enlarges the linear viscoelastic region and enables the fabrication of patterns that have high shape fidelity. Notably, thixotropy, the recovery property of rheology of fluids or gels after removing applied shear forces, critically influences the printing dynamic process after extrusion such as layer-stacking, but its characterization by the three-interval thixotropy test (3ITT) is lacking for PEDOT:PSS-based inks.

Photopolymerization properties for light-based printing. Photopolymerization describes the dynamic transformation of photosensitive precursor inks on exposure to light irradiation and is mainly dependent on three aspects: irradiation wavelength, irradiation energy and photo-gelation time.

When exposed to irradiation with a specific wavelength, photoinitiators first produce active species and then initiate the polymerization. Typical maximal absorption wavelengths of photoinitiators used for compositing PEDOT:PSS are in the near-ultraviolet range (Fig. 3h). To optimize polymerization efficiency, the wavelength used in the printing process should be equal to the maximal absorption wavelength of the photoinitiators[98]. However, according to the Beer–Lambert law[99], absorption in PEDOT:PSS competes with absorption by the photoinitiators. This absorption competition effect varies with wavelength and intensifies in ultraviolet wavelengths:

$$\log_{10}\left(\frac{I_0}{I}\right) = (a_m c_m + a_a c_a) l, \quad (1)$$

in which I_0 and I are the intensities of the incident beam and transmitted beam at a particular wavelength, a_m and a_a are the absorptivities of the matrix and absorber, c_m and c_a are the concentrations of the matrix and absorber and l is the path length related to the printed single-layer thickness. To reduce this competition effect, irradiation wavelengths are commonly shifted from the theoretically optimal wavelengths for printing[36,80,89,100,101] (Fig. 3h). Furthermore, a red shift to longer wavelengths (>405 nm) means that PEDOT:PSS can also be used as a scaffold to carry bioactive tissues and biomaterials in biological and medical applications, as visible light is more compatible with biological tissues[102].

Irradiation energy can influence absorption intensity, energy consumption and thermal instability in the printing process[36]. Notably, a higher irradiation energy leads to a lower absorption intensity (Fig. 3i). However, this effect still lacks intensive studies and is associated with additional requirements for the optimization of printing parameters and for the dynamic modelling of the photopolymerization process.

After absorbing light irradiation, precursor inks start the sol–gel transition (Fig. 3j). On the basis of photopolymerization reaction kinetics and photo-rheology[103], the time to reach the gel point $t_{gel} = \{t: G' = G''\}$ decides the printing speed and shape fidelity. This property is convenient for comparing printability across different photopolymerizable inks.

After printing a bottom layer, the printing platform moves to polymerize another layer, inducing a fluid flow of the precursor ink, on top of the preceding one. Hence, a moderate viscosity (0.25–10 Pa s) is essential for the flowability of precursor inks in light-based printing[104].

Despite recent advances in printable ink designs and printability evaluation, long-term stable printability requires intensive reports and investigations[85]. Such stability ensures a printable window period and the necessary consistency to fabricate reliable printed structures, which will accelerate the translation to commercial productization.

Nozzle-based printing

Meniscus-guided printing. MGP allows the fabrication of high-resolution 3D filament architectures by micropipettes while consuming only microlitres of inks[105]. This technique enables the printing of high-aspect-ratio pillar-like devices in one step.

Generally, MGP allows the fabrication of continuous 3D structures through two alternate processes at the nozzle–substrate interface. One process involves a liquid-to-solid phase transition accompanied by pulling motions, whereas the other process capitalizes on ink meniscus formation introduced by interfacial contact. To expand applicable ink materials, many efforts have been devoted to exploring novel mechanisms for the liquid-to-solid phase transition in MGP. Initially, the phase transition is triggered by electrodeposition inside the meniscus formed by electroplating solutions. This transition uses a two-electrode configuration for electroplating metals but achieves poor control on gelation reactions[106]. Further modifying the printing nozzle into a counter and a reference electrode has enabled PEDOT-based gels with controllable reaction rates[41]. Solvent evaporation was first introduced in 2012 to induce phase transitions for printing PEDOT:PSS[107] (Fig. 4a). This principle enabled liquid-to-solid phase transitions by simply heating rather than polymerization, paving the way for the diversification of the polymer inks offerings.

However, the micropipettes require precise positional feedback during the printing process. This requirement increases the cost of the printing equipment and limits parallel fabrication. Glass micropipettes are fragile and necessitate positional feedback to avoid physical contact with the substrate. To avoid this limitation, an electrohydrodynamic (EHD) dispensing technique introduced electrostatic attractions between the ink and the substrate to create a meniscus at the

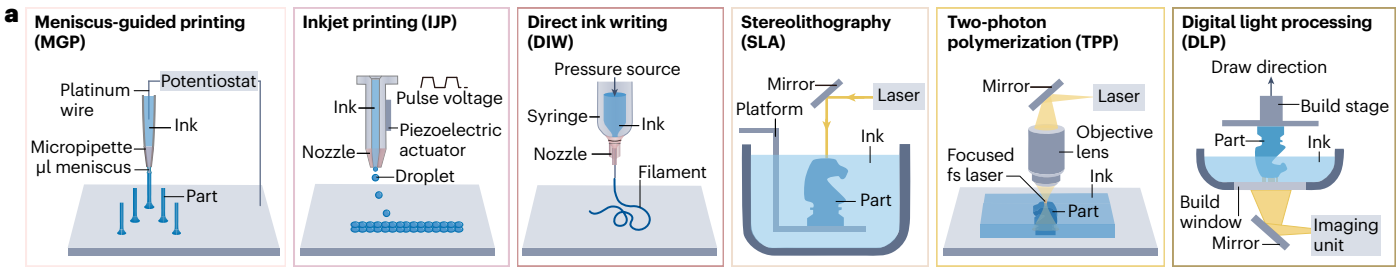

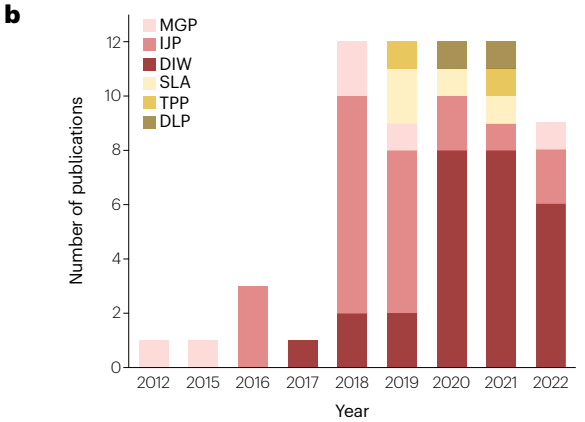

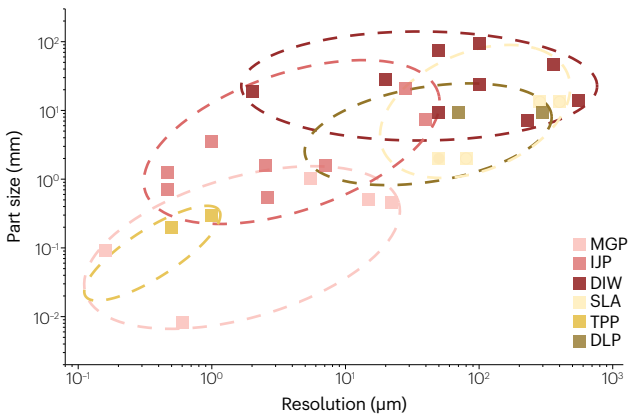

Rheological properties for nozzle-based printing

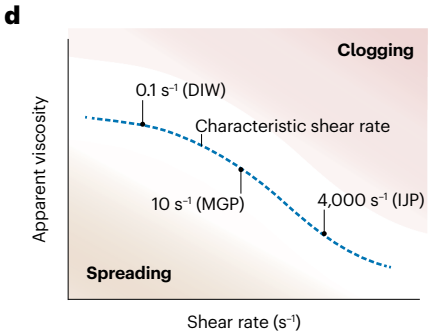

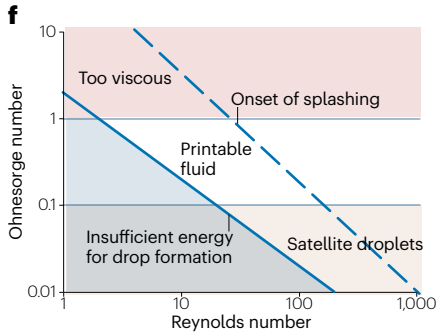

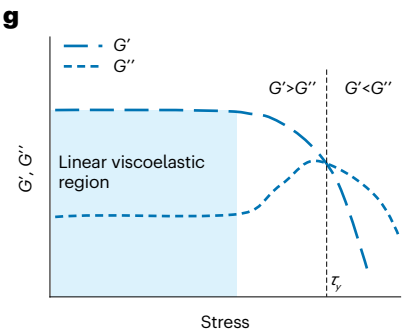

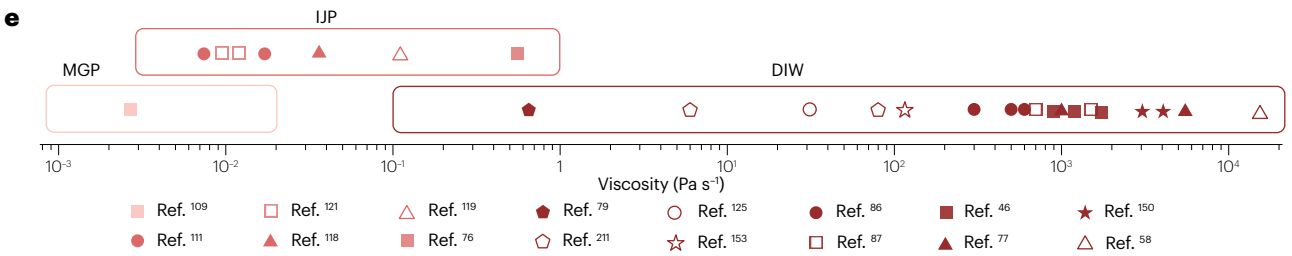

Photopolymerization properties for light-based printing

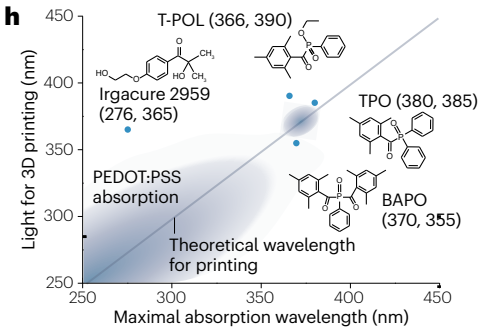

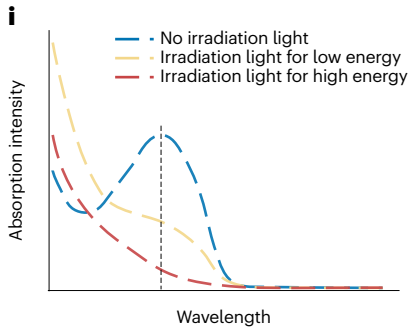

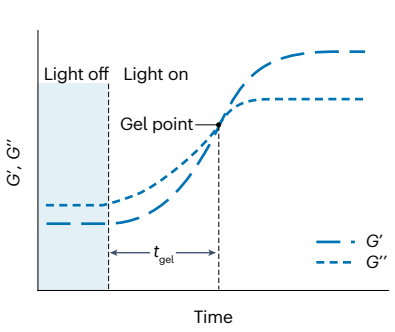

Fig. 3 | Brief overview and printability requirements of typical nozzle-based and light-based printing for poly(3,4-ethylenedioxythiophene):polystyrene sulfonate-based inks. a, Printing mechanisms. **b**, Recent trend in publications on different printing techniques. Data from Web of Science (January 2023). **c**, Comparison of technical characteristics in terms of printed part size and resolution. Circled areas illustrate general printing ability and plotted markers represent specific poly(3,4-ethylenedioxythiophene):polystyrene sulfonate (PEDOT:PSS)-based examples. **d**, Shear-thinning properties of printable inks with characteristic shear rates in correspondent nozzle-based printing. **e**, Typical apparent viscosities of printable inks. The coloured bars illustrate three partially overlapping viscosity ranges, which, respectively, correspond to meniscus-guided printing (MGP), inkjet printing (IJP) and direct ink writing (DIW) processes in nozzle-based printing, and the inserted markers exhibit specific PEDOT:PSS-based printable inks. **f**, Printable fluid window in IJP process with the Ohnesorge and Reynolds numbers. **g**, Shear-yielding properties of printable inks with shear yield stress. **h**, The printing wavelength shifts from the maximal absorption wavelength of the photoinitiators owing to absorption competition from the PEDOT:PSS matrix. **i**, The absorption spectrum of PEDOT:PSS inks varies with the printing irradiation energy. **j**, Photopolymerization kinetics of the sol–gel transition with the time to reach the gel point. BAPO, bis(2,4,6-trimethylbenzoyl)-phenylphosphineoxide; G', storage modulus; G'', loss modulus; TPO, 2,4,6-trimethylbenzoyl-diphenylphosphine oxide; T-POL, ethyl (2,4,6-trimethylbenzoyl) phenylphosphinate. Panel **d** partly adapted from ref. 46, CC BY 4.0. Panel **f** adapted with permission from ref. 93, AIP Publishing. Panel **i** adapted with permission from ref. 36, AAAS.

pipette–substrate gap (~3 μm)[108]. In addition, to create microlitre-sized meniscus, an accurate control of the pulling speed is required (for example, 0.5–2 μm s^{-1}). Pulling the micropipette too fast may separate the ink meniscus from the printed solid phase, but a movement that is too slow might clog micropipettes. Both speeds may fail at printing high-aspect-ratio pillars by serial fabrication. Thus, printing dynamic models have been developed to enlarge the printable window and to improve the fabrication yield of ultrahigh-aspect-ratio (>700) PEDOT:PSS pillars[65,109].

MGP enables the fabrication of filaments by precise pulling-up. The large specific surface area of filaments could provide rapid stimuli-response and surface reactions to printed devices. Outstanding high-aspect-ratio structures are beneficial to the high-density integration of microneedle arrays and to fibre-like bionic devices.

Inkjet printing. The IJP technique uses piezoelectric oscillation or thermal foaming to jet precursor inks into discrete droplets, which subsequently merge and level into printed shapes under the action of surface tension and viscous cohesion[110]. This low-cost technique has enabled the fabrication of PEDOT:PSS-based thin-film patterns such as dots[111], wires[112] and squares[113]. However, expanding the printing to the third dimension remains challenging owing to the trade-off between droplet control and deposition thickness.

Low-viscosity inks (<0.04 Pa s) commonly exhibit strong surface tension (20–70 mN m^{-1}) owing to numerous hydrogen bonds[114]. These inks are easily usable in inkjet printing, but their low cohesion and corresponding levelling limit of single-layer thickness (typically <5 μm) weaken support for the droplets that form the next layer (total <20 layers)[115]. To solve this problem, reactive IJP introduces in-flight microreaction vessels to coalesce gel droplets of PEDOT:PSS and ionic liquids after jetting (within 0.4–0.8 ms), substantially increasing the thickness (~50 μm per layer)[116,117]. Additionally, levelling causes low shape fidelity and uncertain printed patterns. One promising approach is to model printing dynamics for the precise control of inkjet flow[110] and printed pixels[118].

On the contrary, high-viscosity inks (0.04–1.00 Pa s) have thick deposition and stable shape fidelity, but require extra driving forces for droplet generation and jet-flow control. EHD jet printing uses a strong electric field to eject high-viscosity inks into tiny droplets[117,119,120] or filaments[74,75]. Typically, this electrostatic field is induced by a constant voltage of several thousand volts between the nozzle and the substrate. Combining electrostatic deflection with EHD jet printing allowed the precise collection of the high-speed jet stream[42] (Fig. 4b). This technique represents an important step towards ultrafast nozzle-based 3D printing.

Another promising route towards the fabrication of 3D structures is in situ conformal printing on 3D-curved substrates[121,122]. Arbitrarily shaped 3D architectures such as fingertips have been printed conformally with PEDOT:PSS inks[123], indicating the immense potential for next-generation anomalous electronics.

IJP technique is readily applicable to devices with dot arrays, such as multielectrode arrays and curved-display devices. Further steps towards dimension-raising IJP may focus on the development of advanced equipment, including field-assisted printing and hybrid 3D printing.

Direct ink writing. DIW is a low-cost technique that involves the extrusion of precursor inks into continuous fibres, followed by their stretching and bending in flight, and finally to their stacking on substrates[48]. DIW requires inks that have typical viscoelastic behaviours (including high viscosity, high shear-thinning and shear-yielding stress and important thixotropy), which provides wide ink compatibility[97].

Commercial PEDOT:PSS dispersions display low shear yield stress and thus uncontrollable rheological behaviour during their processing (for example, during their lateral spreading on substrates). To inhibit the spreading-out behaviour, a widely used printing strategy consists in compositing commercial dispersions into engineered printable inks as conductive additives[74,78,124]. A milestone method enabling the preparation of pure PEDOT:PSS inks consists in the lyophilization and re-dispersion of PEDOT:PSS[46], enabling the printing of conducting polymer-based microstructures with overhanging features (Fig. 4c). In addition, extruded inks swell up to fibres with a cross-section that is greater than the cross-section of the die (a phenomenon known as die-swelling or the Barus effect), which limits the fabrication resolution (>100 μm)[86]. Modelling the printing dynamics of the viscoelastic inks can offset die-swelling, enabling the fabrication of high-resolution (or even super-resolution) architectures. One promising strategy is to rationally select a nozzle speed V^* (that is, the ratio of extrusion rate to the platform moving speed) and stretch the extruded ink before deposition[78,85,125]. As shown in the following dynamic model, harnessing in-flight ink deformation enables ultrathin fibres with submicron diameter[64]:

$$d = \alpha D/\sqrt{V^*}, \quad (2)$$

in which d and D are the diameters of the printed lines and of the nozzle, and α is the die-swell ratio.

To fabricate 3D structures that are stable long term, deposited PEDOT:PSS-based inks require a robust polymer network, although

thixotropy assists viscoelastic recovery during the DIW process. Typical post-printing crosslinking approaches include light crosslinking[43,126], coagulation baths[58,124] and freeze–thawing[44,85]. Light crosslinking enables the rapid gelation of the extruded inks using photochemical reactions, but adding photosensitive additives may weaken the contribution of PEDOT:PSS to the electrical and mechanical properties of the ink and even introduce cytotoxicity[127–129]. Coagulation baths crosslinking harness ions or surfactants in reservoirs to break the Coulombic

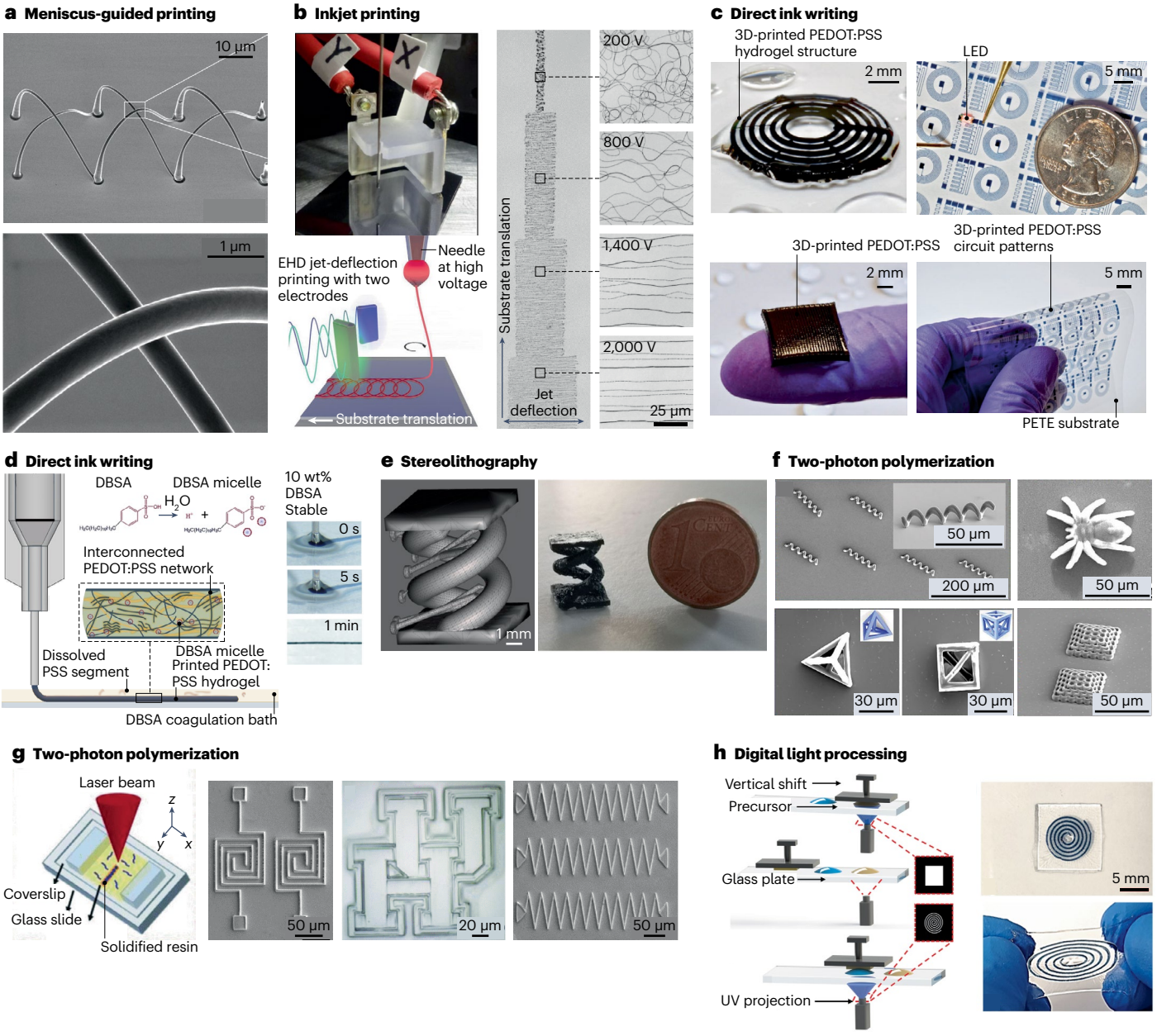

Fig. 4 | Nozzle-based and light-based printing techniques. a, Meniscus-guided printing: 3D poly(3,4-ethylenedioxythiophene):polystyrene sulfonate (PEDOT:PSS) mechanical buckling arrays with high stretchability (>270%) for electrical interconnection. **b**, Inkjet printing: electrohydrodynamic (EHD) 3D printer with jet-deflecting electric field-printed poly(ethylene oxide)-PEDOT:PSS in an ultrafast controllable way. **c**, Direct ink writing: extruded pure PEDOT:PSS for the fabrication of overhanging and scalable structures. **d**, Direct ink writing: 4-dodecylbenzenesulfonic acid (DBSA)-based coagulation bath induces the rearrangement of PEDOT chains. **e**, Stereolithography: digital-customized double helical-shaped PEDOT:PSS polymers. **f**, Two-photon polymerization (TPP): micrometre-scale 3D architectures by in situ self-assembly. **g**, TPP: direct TPP of PEDOT:PSS-based zig-zag and coil-like arrays. **h**, Digital light processing: multimaterial printing for hydrogel–elastomer hybrid structures. LED, light-emitting diode; PETE, polyethylene terephthalate; UV, ultraviolet. Panel **a** reprinted with permission from ref. 108. Copyright 2012 American Chemical Society. Panel **b** reprinted from ref. 42, CC BY 4.0. Panel **c** adapted from ref. 46, CC BY 4.0. Panel **d** reprinted with permission from ref. 58, Wiley. Panel **e** reprinted from ref. 135, CC BY 4.0. Panel **f** reprinted with permission from ref. 139, Royal Society of Chemistry. Panel **g** reprinted with permission from ref. 102, IEEE. Panel **h** reprinted with permission from ref. 101. Copyright 2021 American Chemical Society.

force between $PEDOT^+$ and PSS^- chains and induce the rearrangement of PEDOT chains for in situ gelation[58] (Fig. 4d). Freeze–thawing builds on reversible physical bonding, allows facile processing and can stabilize the as-formed polymer network for further treatments[44,85]. In brief, post-printing treatments can endow 3D-printed structures with good shape fidelity, higher mechanical and electrical performance as well as better structural reliability[69,130,131].

The DIW technique facilitates the fabrication of fractal lattices, in-tubule stents and blood vessel-like wires. This technique also has outstanding ink compatibility, enabling the continuous extrusion of multimaterial inks for all-printed electronics and robotic systems, whereas the printed polymers have sufficient mechanical strength to form complex 3D structures such as hollowed areas, overhanging frameworks and other 3D entities.

Light-based printing

Stereolithography. The SLA technique allows the selective photopolymerization of inks by focusing a laser facula. PEDOT:PSS-PEGDA inks are one of the most commonly used precursors for photopolymerization[89,132]. The composition and the proportion of the components of the inks affect both the printing performance (such as transparency and crosslinking efficiency) and the properties of the polymer[90]. Additionally, the laser power and scanning speed determine the exposure time and irradiance[133]. Overexposure negatively impacts shape fidelity and manufacturing speed. By optimizing the aforementioned printing parameters, complex PEDOT:PSS-PEGDA architectures such as ring chains and 3D double helical-shaped structures could be fabricated[90,134] (Fig. 4e). To date, SLA has enabled the fabrication of 3D structures with complex topology and large-format patterns. Further combination with experimental design will lead to more comprehensive and effective printing parameter optimization.

Two-photon polymerization. The TPP technique uses two-photon absorption to achieve the highest resolution among 3D-printing technologies[135]. However, the direct TPP of conducting polymers is limited by the strong absorption of polaron carriers in the visible and near-infrared regions[136]. Incipient routes commonly focus on a two-step strategy combining TPP with in situ oxidative polymerization[137] or self-assembly[138] (Fig. 4f). Although these strategies enable the fabrication of complicated architectures from conducting polymers, the resultant low conductivity limits their practical applications[138]. The first TPP-fabricated PEDOT:PSS-photopolymer ink with both outstanding resolution (~2 μm) and high conductivity (281 S cm^{-1}) was demonstrated in 2021 (ref. 101) (Fig. 4g).

Although the very high resolution attainable with this technique enables the fabrication of small structures, such as implantable robots for tubular organs, the associated high operation costs and limited fabrication rates still confine TPP at the laboratory scale. Integrating equipments such as digital micromirrors with the TPP platform can enable multifocus scanning towards parallel and scalable manufacturing[139]. There are two commonly used strategies for parallel processing on the basis of micromirrors. First, including one microlens array in the light path enables to split the laser focus into multiple foci. Second, by combining digital micromirror devices with a spatially and temporally focused laser, one can generate a patterned light sheet.

Digital light processing. The DLP technique uses digital light projectors rather than point-source irradiation for exposure. Because it can print in parallel, DLP has fast printing speeds. However, the technique necessitates the use of micromirror arrays, which limits the process area[140,141]. Moreover, DLP enables the precise spatial and temporal control of the polymerization as well as better shape fidelity and higher reproducibility than nozzle-based printing[142]. As an example, PEDOT:PSS-acrylamide inks for cross-scale hydrogel–elastomer hybrid devices could be printed with a resolution of 70 μm (ref. 100) (Fig. 4h). Incomplete photopolymerization also leads to strong interfacial bonding between the device and the substrate[100].

DLP can enable the rapid fabrication of complicated architectures and array structures, which pave the way for 3D metamaterials and structure engineering towards the exploration of properties and capabilities beyond those of bulky ingredient materials.

Applications in soft robotics

PEDOT:PSS can be in both dry and hydrogel states owing to the strong hygroscopicity of PSS. Although dry PEDOT:PSS-based materials are definitely promising candidates in soft robotics owing to their high electrical conductivity, their hydrogels face several challenges including insufficient reliability in air resulting from water loss and temperature instability. Strategies such as encapsulation or incorporating humectants need to be further explored to overcome such drawbacks. On the contrary, PEDOT:PSS-based hydrogels do have unique advantages in wet environments, making them suitable for implantable medical soft robots and subaqueous robotic systems.

Soft bioelectronics

Soft bioelectronics hold promise for the fabrication of stable human–robot interfaces that are associated with less tissue damage and reduced motion artefacts in electrophysiological signals[143]. Three-dimensional-printed PEDOT:PSS has emerged as a promising candidate offering biocompatibility and good conformality for applications ranging from the cellular level to organs[31,45,46,58,74,144].

Artificial extracellular matrices. The extracellular matrix affects fundamental cellular processes through mechanosensitive proteins and ion channels[145]. Simulating the viscoelastic behaviours of the natural matrix is essential for biomedical applications such as drug delivery and regenerative medicine[146] (Fig. 5a). Three-dimensional-printed PEDOT:PSS hydrogels exhibit tunable mechanical properties, enabling the matching of its mechanical properties with the extracellular matrix and tissues[124]. The further customization of the molecular network of PEDOT:PSS hydrogel and 3D geometry allows long-term organoid culture in vitro[147,148].

Typically, PEDOT:PSS acts as a conducting additive in artificial extracellular matrices to induce the directional arrangement of cultured living cells[74] and for growth[149] and differentiation[62,89]. For example, by using EHD printing techniques, anisotropic culture lattices of PEDOT:PSS-PEO have been fabricated to mimic the hierarchical microstructure of native myocardium tissues[74] (Fig. 5a). Additionally, 3D-printed PEDOT:PSS could form multimaterial 3D frameworks for the culture of cells at specific sites in applications such as segmental tissue reconstruction of the trachea and myofibres.

Bioelectronic interfaces. Bioelectronic interfaces can stimulate biological tissues and record neural activities using electrical signals[128,150] (Fig. 5b). The mixed ionic and electronic conductivity of PEDOT:PSS provides low interfacial impedance, strong ion-injection ability and low operation voltage[151,152], allowing ionic communication for fully implantable devices[144]. Furthermore, printing methods that use multimaterials

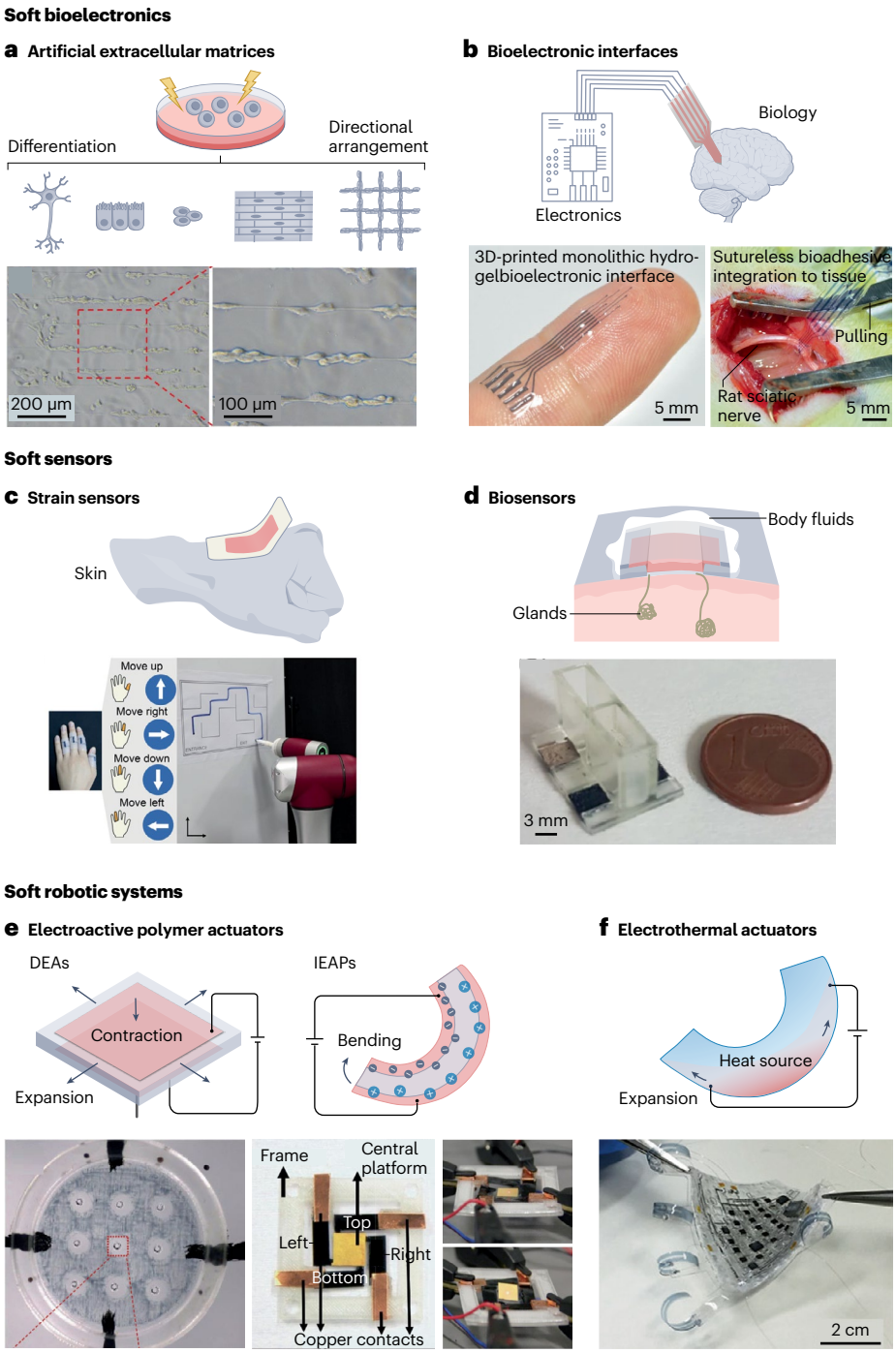

Fig. 5 | Three-dimensional-printed poly(3,4-ethylenedioxythiophene):polystyrene sulfonate for soft robotics. a, Bioelectronics: artificial extracellular matrices for cell cultures and examples of myocardium tissues mimicking for inducing cell arrangement. **b**, Bioelectronic interfaces: bridging the interface between biology and electronics and examples of monolithic all-hydrogel bioelectronic interfaces with sutureless adhesive to rat tissues. **c**, Patch-like printed poly(3,4-ethylenedioxythiophene):polystyrene sulfonate for on-skin detection and examples of universal electronic skins for human–robot interfaces. **d**, Thin-film organic electrochemical transistors for body-fluid sensing and examples as 3D-printed organic electrochemical transistor with 700-μm wide channel. **e**, Electroactive polymer actuators, including dielectric elastomer actuators (DEAs) and ionic electroactive polymer actuators (IEAPs), and examples of transparent tunable acoustic absorber membranes as well as monolithic soft parallel manipulators with three degrees of freedom. **f**, Electrothermal actuators and examples of fully soft robotic systems integrating electronic skins and humanoid hand actuators. Panel **a** partly reprinted with permission from ref. 75, Royal Society of Chemistry. Panel **b** partly reprinted from ref. 45, Springer Nature Limited. Panel **c** partly reprinted with permission from ref. 44, Wiley. Panel **d** partly reprinted from ref. 133, CC BY 4.0. Panel **e** partly reprinted with permission from ref. 120, Copyright 2018 American Chemical Society, and ref. 178, Elsevier. Panel **f** partly reprinted with permission from ref. 40, AAAS.

can be used to fabricate monolithic bioelectronic interfaces continuously, reducing the time and cost for mass personalization[58]. However, conducting polymers inherently lack stable interfacial adhesion with wet tissues. This deficiency harms signal-to-noise ratios and limits the long-term electrophysiological recording and stimulation of various organs. Improving adhesion can be done throughout the whole production process, for example, by compositing supramolecular solvent during ink design[153], integrating bioadhesive hydrogels during fabrication[45] or weakening hydrogen bonding between the PSS and water during post-treatment[58]. As an example of a fully printed all-hydrogel bioelectronic interface, monolithic bi-continuous PEDOT:PSS-PU hydrogels with high stretchability (>400%) and stable electrical properties (over 10,000 charging and discharging cycles) were fabricated in less than 10 min (ref. 45) (Fig. 5b). The printed hydrogel also demonstrated excellent long-term stability (in terms of conductivity, ultimate strain and toughness) in physiological environments and enabled rapid, robust

and sutureless bio-interfacing with tissues and organs such as the heart, sciatic nerves and spinal cords over 2 months[45].

Soft sensors

Strain sensors. Strain sensors are fundamental in human–robot interactions and are generally arranged on human or robotic skins to detect local deformation[154] (Fig. 5c). Currently, PEDOT:PSS enables the monitoring of cross-scale deformations from slight vibrations (such as pulse, pitch and pat) to vigorous motions (such as flexing joint and pneumatic inflation)[43,103]. A patch-like configuration coupled with its intrinsic flexibility endows PEDOT:PSS with mechanical compliance to skins. However, because human and robotic skins have different motion behaviours, dissimilar properties for PEDOT:PSS-based strain sensors are needed. Owing to the musculoskeletal systems and skin texture, human skins generally exhibit non-uniform and nonlinear behaviours during local deformation. These features require ultrahigh compliance or printed anchor structures for conformal contact[43,155]. On the contrary, soft materials for robotic systems are commonly homogeneous and smooth, which facilitate mechanical properties matching for on-skin sensors. In addition, multimodal sensing can contribute to the elaboration of more versatile robotic systems. Three-dimensional-printed PEDOT:PSS has been used to construct pyramid microstructures for strain isolation[100] as well as laminated arrays for multipixel perception[121,156]. To construct a universal strain sensor, PEDOT:PSS-PVA hydrogels with a microphase semiseparated network were printed[44]. Their stable cycling stretchability (100% strain for 2,000 cycles) and low hysteresis (<1.5%) could reliably capture hand gestures to control an industrial robotic arm, and the robust resistance to off-axial deformations could provide objection recognition for a soft gripper[44] (Fig. 5c).

Biosensors. Soft biosensors enable the rapid, in situ and long-term monitoring of biomarkers in body fluids such as sweat and blood[157,158]. High-gain biosensors provide the necessary sensitivity for health monitoring and disease screening[159]. As one promising alternative, organic electrochemical transistors (OECTs) use a semiconductor channel that receives ions from body fluids and then modulate their bulky conductivity to output the drain current as sensing signals[160] (Fig. 5d). Mixed ionic and electronic doping charges over the entire channel give OECTs outstanding theoretical transconductance. Their high current ON/OFF ratio (>10^3), low-voltage operation (<1 V) and facile integration also make them particularly suitable for applications in fully printed soft logic circuits, for example, as flexible inverter logic gate sensors for inferring cation types[160,161]. To date, PEDOT:PSS has been widely used for the channel owing to its nanoporous conductive matrix and accompanying high volumetric capacitance[162,163]. These features facilitate the creation of an electrical double layer (acting as a capacitor) for efficient electron-ion transduction while in operation[151]. However, there are no appropriate inks designed for PEDOT:PSS-based OECTs, and compatible fabrication techniques for thick channels are lacking, which lessens their practical transconductance. Typically, the thickness of the channels is less than 10 μm owing to the low viscosity of the PEDOT:PSS aqueous dispersion and the technique used (IJP)[122,161]. However, PEDOT:PSS-PEGDA inks have been composed to fabricate thick channels (~500 μm) by SLA (Fig. 5d), which resulted in the highly sensitive detection (4.4 μM) of dopamine[132].

Soft robotic systems

Three-dimensional-printed PEDOT:PSS can be used to fabricate actuators, such as electroactive polymer actuators (EAPs) and electrothermal actuators (ETAs), in soft robotics. For these applications, PEDOT:PSS stores input electric energy as the electrostatic field or converts it into joule heat for powering operations.

Electroactive polymer actuators. EAPs harness the converted electrostatic field for actuation and can be roughly subdivided into dielectric elastomer actuators and ionic electroactive polymer actuators (IEAPs) according to the type of electrostatic interaction[164] (Fig. 5e).

Dielectric elastomer actuators utilize electrostatic forces to compress an insulating elastomer sandwiched between two electrodes. They have been widely used in artificial muscles owing to their large actuation strain, high operating frequency and low cost[165,166]. Compared with carbon-based materials, PEDOT:PSS is outstandingly processible and can form uniform thin-film electrodes. Such an advantage enables its use in transparent optical tunable devices such as smart windows[167,168], soft lenses[169] and camouflage robots[170] with good reliability (typically >1,000 cycles). Further combination with on-demand printing facilitates the configuration of sophisticated robotic systems. For example, printed transparent acoustic absorbers with a contractible hole diameter demonstrated a tunable frequency spectrum and broad absorption bandwidth (444 Hz)[119] (Fig. 5e).

IEAPs consist of two polymer electrodes and an electrolyte membrane in a sandwich-like structure. Ions within the electrolyte are inserted and/or extracted in or from the electrodes under an electric field and thus induce an asymmetrical volume change for bending[171]. This actuation mechanism gives IEAPs low activation voltage, large bending displacement and bidirectional actuation[172]. One merit of using PEDOT:PSS as the electrode is that inks can be blended with conductive fillers to improve actuation performance[173,174]. Furthermore, PEDOT:PSS can be used to construct interpenetrating polymer networks at electrode–electrolyte interfaces, improving durability[175]. However, because of the sandwich-like structure, the actuation mode is constrained to bending, which further limits practical applications in soft robots needing multimodal actuation. Integrating multiple actuators is one promising route towards complicated functions such as flapping in bionic dragonflies[176], in which IJP techniques have been used to tailor PEDOT:PSS electrodes in actuators. As an example, a monolithic manipulator platform with four IEAPs in a circle arrangement[177] (Fig. 5e) enabled three motion degrees to operate four-way laser steering.

Electrothermal actuators. ETAs utilize embodied flexible conductors to locally heat electrothermal-responsive polymers (such as polydimethylsiloxane or poly(lactic acid)) for asymmetrical thermal expansion[178] (Fig. 5f). So far, they have been used in grippers, chromatic displays and biomimetic robots with the merits of delivering a high output force and being lightweight and electrolyte-free[82,178,179]. By using an electrothermomechanical lumped element model, deformation can be predicted, which enables accurate manipulation in microcellular surgery[180,181]. However, one of the grand limitations for PEDOT:PSS-based electrothermal actuators is the long actuation period owing to the following two factors[178]. First, inefficient electrothermal conversion dissipates considerable electrical and thermal energy and limits the activation speed. This issue also causes extra driving voltage and narrows the application scope. One promising route is to shorten the conduction distance and construct distributed heating networks such as core-sheath structures by coaxial extrusion[43]. Second, the limited specific surface area weakens heat convection for cooling and delays the recovery time. Owing to the film-forming properties of PEDOT:PSS, an ultrathin ETA (~200-μm thickness) was printed, which

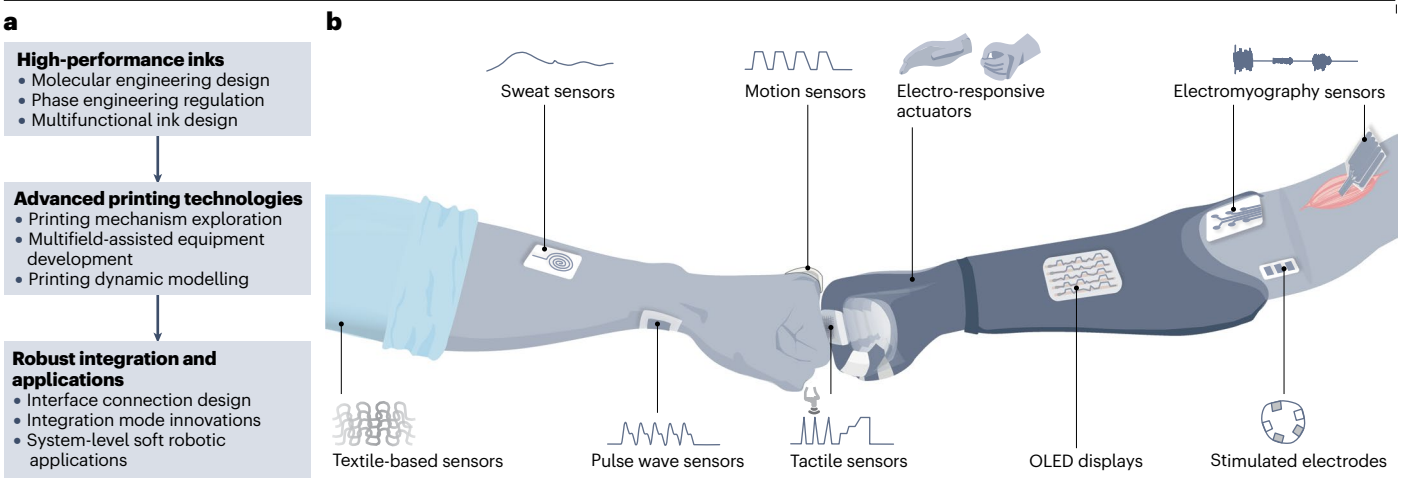

Fig. 6 | Perspectives. a, Future directions for 3D-printed poly(3,4-ethylenedioxythiophene):polystyrene sulfonate. **b**, Perspective applications in soft robotics. OLED, organic light-emitting diode.

had a fast actuation period (<20 s) and low drive voltages (0–15 V)[40] (Fig. 5f). Its further integration with electronic skins provided wireless activation for fully soft and skin-like robotic hands[40].

Future perspectives

As an interdisciplinary product, 3D-printed PEDOT:PSS has shown its unique role in soft robotics for human–robot interaction applications. Three-dimensional printing provides PEDOT:PSS-based materials with expansive design space and task-specific fabrication, and PEDOT:PSS inspires novel printing mechanisms and manufacturing facilities. Currently, 3D-printed PEDOT:PSS for soft robotics is still at the laboratory stage, in which opportunities and challenges remain (Fig. 6a).

High-performance ink design

The rational design of multifunctional inks that have, in particular, satisfactory electrical, mechanical, biological or optical properties is an important future research direction to fulfil the varying practical requirements of soft robotic systems. Future high-performance PEDOT:PSS inks should aim to decouple compositing-induced compromises among printability, polymer properties and long-term stability through multiscale design strategies.

Molecular engineering design. The abundant chemical moieties on PEDOT:PSS provide opportunities for systematically designing and modifying the molecular structures of PEDOT and PSS segments. Chemical functionalization of PEDOT segments (by introducing dynamic covalent bonds, side chains, soft segments or hydrophilic groups, for example) can give PEDOT segments diverse intrinsic properties, such as solubility, flexibility, fast interchain charge transfer and high charge carrier density[182]. Alternatively, the aqueous dispersibility of PSS chains enables the application of diverse molecular modification towards smart soft materials. Adding functional groups on PSS chains could simultaneously endow PEDOT:PSS inks with multiple sophisticated properties such as fatigue resistance, adhesion, antifreezing, antidehydration and stimuli response.

Phase engineering regulation. Currently, phase separations in printed PEDOT:PSS rely on post-treatments with complex procedures. Pre-formed phase separations of PEDOT and PSS domains and of PEDOT:PSS and other materials in precursor inks may improve multiple properties simultaneously, such as seen in solubility-induced phase separation leading to bi-continuous phases with good electrical and mechanical properties. Phase engineering of the inks at varying length scales, ranging from the atomic/molecular level to the nanoscale, microscale and macroscopic levels, can have a crucial role in maximizing the performance of 3D-printed PEDOT:PSS. Regulation strategies involving ink formulation, solvent engineering, additive and dopant selection, post-processing techniques and even computational modelling should be developed for soft robotic applications in the future.

Multifunctional ink design. The rational design of multifunctional PEDOT:PSS-based inks is still critical to advance this young field. By resorting to varying design strategies such as molecular functionalization, doping, nanostructuring, hybridization or compositing, multifunctional PEDOT:PSS-based inks may provide the printed structures with improved electrical, mechanical, biological, interfacial as well as optical, thermal, magnetic and acoustic properties. The broad diversity of material options as well as manageable molecular compositing techniques suggest a bright future for this direction.

Advanced printing technologies

The outstanding water dispersibility of PEDOT:PSS makes its formulations low cost, biocompatible and printable, but is also associated with lingering challenges during the printing of 3D structures, such as limited shape fidelity and phase separation, owing to the migration of solute polymer induced by undesired solvent flow. Future developments in advanced printing technologies are expected to address these issues through mechanism exploration, equipment development and dynamic modelling.

Printing mechanism exploration. One promising route is to explore alternative 3D printing technologies, such as fused deposition modelling and selective laser sintering, that are based on PEDOT:PSS solids. However, these techniques rely on local heating to pattern thermoplastic solids and usually lead to previous irreversible oxidation or to the decomposition of PEDOT:PSS[183]. To alleviate this issue, compositing

PEDOT:PSS-based conducting polymers into engineered precursors that have low melting temperatures, such as paraffin and ethylene-vinyl acetate copolymer, is an obvious direction[184]. Combining this strategy with molecular engineering may further retain the intrinsic flexibility and conductivity.

Multifield-assisted equipment development. Multifield-assisted equipments, which are printing platforms surrounded by physical fields such as displacement, electric, magnetic or acoustic fields, endow extra design freedom to 3D printing. Interestingly, introducing a displacement field (for example, by using robotic arms with six-axis control[185] or autonomous robots[186]) greatly expands the workspace of the printhead and enables in situ printing for conformal electronics. Assistance from physical fields (such as electric, magnetic or acoustic fields) enables the printing of anisotropic architectures with reconfigurable programming, such as directional freezing for hierarchical structures[187,188].

Printing dynamic modelling. Modelling printing dynamics helps in improving the resolution, predictability, consistency and reliability of printed structures. Although persistent efforts have been focused on modelling passive materials (such as polymers or resin)[125,189], modelling the printing dynamics of conducting polymers is challenging because the rigidity of conducting polymer chains is greatly different from that of passive materials[190]. Additionally, aqueous dispersions of conducting polymers are richer in non-covalent interactions such as π–π stacking and hydrogen bonding[191]. The resultant high surface tension may trigger spontaneous flow and further printing failures such as levelling and structure collapse. All these factors complexify the dynamic modelling and demand collaborative efforts from rheology, soft matter mechanics and polymer physics.

Robust integration and applications

Interface design. Interfaces bridge multimaterial components within the robotic system and merge soft robots with target environments. Interface designs, using, for example, topological bonding and intermolecular bonding, have attracted much attention[192,193]. However, taking soft hybrid devices as an example, it is still very challenging to design reliable interfaces between hydrogels and elastomers under stretching conditions. By contrast, mechanical interlocking, which creates mutual physical dependence between distinct components, has broad applicability for materials, and multimaterial 3D printing can be used to fabricate interlocking architectures that are continuously integrated across interfaces. However, merging robots and humans requires stable interfaces that are tough, exhibit low impedance and have tunable functionality. Bridging conducting polymers with wet biological tissues or rigid external equipment remains a typical challenge in the field, owing to the hysteresis, limited applicability and mechanical mismatch of mature elastomeric binders[194–196]. Specifically, the hysteresis introduced by adhesions will distort signals in the detection and tactile feedback of high-frequency vibrations. Restricted applicability also complexifies the formulation of hybrid devices and limits interactions with subaqueous environments.

Integration mode innovations. Integration modes define how different parts are assembled. Three-dimensional-printed PEDOT:PSS is usually covered by soft encapsulation layers to form a sandwich-like structure and then can be attached to robots or humans as independent components. The advantage of this integration mode is that components are interchangeable, but it generally demands extra fabrication and assembly procedures[197,198]. Embedded 3D printing uses bodies of soft robots as substrates to encapsulate conductive materials, enabling embodied intelligence at a low cost with good product consistency and reliable interfaces[199]. Other integration modes, for which multimaterial printing is one promising and essential tool, still require extensive investigation. For example, printing stimuli-responsive materials into air chambers renders pneumatic fibre-like robots autonomous in confined environments[200]. Additionally, in situ printing provides possibilities for retrofitting existing devices or functionalizing living tissues.

System-level soft robotic applications. Three-dimensional-printed PEDOT:PSS brings innovations at the mechanism, device and system scale in soft robotics (Fig. 6b). The mixed ionic and electronic conductivity of PEDOT:PSS inspires high-performance tactile sensing using novel mechanisms[201,202]. Furthermore, 3D-printed PEDOT:PSS can increase the dimensionality of displays, perception and data processing in soft robots to three dimensions (as exemplified by six-axis force and/or torque sensors and 3D logical circuits[6,18,203]). For robotic systems, soft-printed electronics based on PEDOT:PSS have emerged as energy-harvesting and conversion systems, functional optoelectronics or artificial synapses[204–207]. All of these examples demonstrate the possibility to be integrated into one untethered and autonomous robotic system rather than being constrained to external equipment.

Because of its electroactivity and low foreign-body response[52], 3D-printed PEDOT:PSS has practical applications in biomedical engineering. In particular, integrating bioelectronics and sensors with soft actuators can enable multifunction medical interventions[208]. For instance, self-sensing soft robots can supplement rigid and abiotic instruments in surgeries such as eye surgeries[209], in which they can apply traction for the orbital adipose tissues with real-time intraocular pressure feedback. Three-dimensional-printed PEDOT:PSS is also an additional tool to develop fully printed microrobots and implantable soft robots such as variable-stiffness robots[210]. Other potential applications for PEDOT:PSS include gas leakage detections and subaqueous liquid exchange, whereas 3D printing could enable the fabrication of bionic structures.

There is a long and challenging history of applying conducting polymers in electronics, in which persistent efforts aim to reduce onboard mechanical fragility and improve conductivity. Interestingly, the development of applications in soft robotics progresses hand-in-hand with our understanding of cross-scale fabrication technologies. Fuelled by advances in PEDOT:PSS inks and 3D-printing techniques, we are moving away from in-device stacking fabrication to integrated manufacturing for intelligent soft robotic systems. In the future, there is no doubt that 3D-printed PEDOT:PSS will face formidable trials and challenges, such as the development of high-performance yet reliable materials, the manufacturing scale-up and integration, the realization of sustained operation in soft robotic applications as well as the exploration of innovative applications, their translation and commercialization. Meanwhile, 3D-printed PEDOT:PSS also provides encouraging promises in soft robotics to seamlessly merge humans and robots.

Published online: 24 August 2023

References

1. Downs, F. G. et al. Multi-responsive hydrogel structures from patterned droplet networks. *Nat. Chem.* **12**, 363–371 (2020).
2. Wu, Y., Dong, X., Kim, J. K., Wang, C. & Sitti, M. Wireless soft millirobots for climbing three-dimensional surfaces in confined spaces. *Sci. Adv.* **8**, eabn3431 (2022).
3. Kim, Y., Parada, G. A., Liu, S. & Zhao, X. Ferromagnetic soft continuum robots. *Sci. Robot.* **4**, eaax7329 (2019).

4. Kim, Y. et al. Telerobotic neurovascular interventions with magnetic manipulation. *Sci. Robot.* **7**, eabg9907 (2022).
5. Gu, G. et al. A soft neuroprosthetic hand providing simultaneous myoelectric control and tactile feedback. *Nat. Biomed. Eng.* https://doi.org/10.1038/s41551-021-00767-0 (2021).
6. Yan, Y. et al. Soft magnetic skin for super-resolution tactile sensing with force self-decoupling. *Sci. Robot.* **6**, eabc8801 (2021).
7. Yao, K. et al. Encoding of tactile information in hand via skin-integrated wireless haptic interface. *Nat. Mach. Intell.* **4**, 893–903 (2022).
8. Barreiros, J. A. et al. Haptic perception using optoelectronic robotic flesh for embodied artificially intelligent agents. *Sci. Robot.* **7**, eabi6745 (2022).
9. Lin, W. et al. Super-resolution wearable electrotactile rendering system. *Sci. Adv.* **8**, eabp8738 (2022).
10. Yun, S. S., Kim, K., Ahn, J. & Cho, K. J. Body-powered variable impedance: an approach to augmenting humans with a passive device by reshaping lifting posture. *Sci. Robot.* **6**, eabe1243 (2021).
11. Proietti, T. et al. Restoring arm function with a soft robotic wearable for individuals with amyotrophic lateral sclerosis. *Sci. Transl. Med.* **15**, eadd1504 (2023).
12. Rus, D. & Tolley, M. T. Design, fabrication and control of soft robots. *Nature* **521**, 467–475 (2015).
13. Zhao, X. et al. Soft materials by design: unconventional polymer networks give extreme properties. *Chem. Rev.* **121**, 4309–4372 (2021).
14. Apsite, I., Salehi, S. & Ionov, L. Materials for smart soft actuator systems. *Chem. Rev.* **122**, 1349–1415 (2022).
15. Cai, M. et al. A multifunctional electronic skin based on patterned metal films for tactile sensing with a broad linear response range. *Sci. Adv.* **7**, eabl8313 (2021).
16. Jiang, Z. et al. A 1.3-micrometre-thick elastic conductor for seamless on-skin and implantable sensors. *Nat. Electron.* **5**, 784–793 (2022).
17. Song, H. et al. Highly-integrated, miniaturized, stretchable electronic systems based on stacked multilayer network materials. *Sci. Adv.* **8**, eabm3785 (2022).
18. Cui, C. et al. Controlled desiccation of preprinted hydrogel scaffolds toward complex 3D microarchitectures. *Adv. Mater.* **35**, e2207388 (2022).
19. Markvicka, E. J., Bartlett, M. D., Huang, X. & Majidi, C. An autonomously electrically self-healing liquid metal-elastomer composite for robust soft-matter robotics and electronics. *Nat. Mater.* **17**, 618–624 (2018).
20. Yeom, J. et al. Soft and ion-conducting hydrogel artificial tongue for astringency perception. *Sci. Adv.* **6**, eaba5785 (2020).
21. Shi, J. et al. Embedment of sensing elements for robust, highly sensitive, and cross-talk-free iontronic skins for robotics applications. *Sci. Adv.* **9**, eadf8831 (2023).
22. Zhao, Y. et al. A self-healing electrically conductive organogel composite. *Nat. Electron.* https://doi.org/10.1038/s41928-023-00932-0 (2023).
23. Jang, S., Shim, H. & Yu, C. Fully rubbery Schottky diode and integrated devices. *Sci. Adv.* **8**, eade4284 (2022).
24. Jiang, Y. et al. Topological supramolecular network enabled high-conductivity, stretchable organic bioelectronics. *Science* **375**, 1411–1417 (2022).
25. He, H. et al. Salt-induced ductilization and strain-insensitive resistance of an intrinsically conducting polymer. *Sci. Adv.* **8**, eabq8160 (2022).
26. Berggren, M. et al. Ion electron-coupled functionality in materials and devices based on conjugated polymers. *Adv. Mater.* **31**, 1805813 (2019).
27. Feig, V. R. et al. An electrochemical gelation method for patterning conductive PEDOT:PSS hydrogels. *Adv. Mater.* **31**, 1902869 (2019).
28. Zhang, S. et al. Room-temperature-formed PEDOT:PSS hydrogels enable injectable, soft, and healable organic bioelectronics. *Adv. Mater.* **32**, 1904752 (2020).
29. Lee, Y. et al. A low-power stretchable neuromorphic nerve with proprioceptive feedback. *Nat. Biomed. Eng.* https://doi.org/10.1038/s41551-022-00918-x (2022).
30. Kim, T. et al. Dynamic tactility by position-encoded spike spectrum. *Sci. Robot.* **7**, eabl5761 (2022).
31. Jiang, Y. et al. Wireless, closed-loop, smart bandage with integrated sensors and stimulators for advanced wound care and accelerated healing. *Nat. Biotechnol.* https://doi.org/10.1038/s41587-022-01528-3 (2022).
32. Xu, C. et al. A PEDOT:PSS conductive hydrogel incorporated with Prussian blue nanoparticles for wearable and noninvasive monitoring of glucose. *Chem. Eng. J.* **431**, 134109 (2022).
33. Bae, E. J., Kang, Y. H., Jang, K. S., Lee, C. & Cho, S. Y. Solution synthesis of telluride-based nano-barbell structures coated with PEDOT:PSS for spray-printed thermoelectric generators. *Nanoscale* **8**, 10885–10890 (2016).
34. Zhu, C. X. et al. Stretchable temperature-sensing circuits with strain suppression based on carbon nanotube transistors. *Nat. Electron.* **1**, 183–190 (2018).
35. Wang, S. et al. Skin electronics from scalable fabrication of an intrinsically stretchable transistor array. *Nature* **555**, 83–88 (2018).
36. Zheng, Y. Q. et al. Monolithic optical microlithography of high-density elastic circuits. *Science* **373**, 88–94 (2021).
37. Yap, H. K., Ng, H. Y. & Yeow, C.-H. High-force soft printable pneumatics for soft robotic applications. *Soft Robot.* **3**, 144–158 (2016).
38. Zhu, Z., Ng, D. W. H., Park, H. S. & McAlpine, M. C. 3D-printed multifunctional materials enabled by artificial-intelligence-assisted fabrication technologies. *Nat. Rev. Mater.* **6**, 27–47 (2020).
39. Cui, H. et al. Design and printing of proprioceptive three-dimensional architected robotic metamaterials. *Science* **376**, 1287–1293 (2022).
40. Byun, J. et al. Electronic skins for soft, compact, reversible assembly of wirelessly activated fully soft robots. *Sci. Robot.* **3**, eaas9020 (2018).
This work demonstrates ultrathin skin-type soft robotic hands on the basis of rapid electrothermal actuation.
41. Da Silva, A. C., Wang, J. & Minev, I. R. Electro-assisted printing of soft hydrogels via controlled electrochemical reactions. *Nat. Commun.* **13**, 1353 (2022).
42. Liashenko, I., Rosell-Llompart, J. & Cabot, A. Ultrafast 3D printing with submicrometer features using electrostatic jet deflection. *Nat. Commun.* **11**, 753 (2020).
This work introduces electrostatic deflection into electrohydrodynamic jet printing and enables ultrafast 3D printing of thin-walled structures.
43. Wei, H. et al. Orthogonal photochemistry-assisted printing of 3D tough and stretchable conductive hydrogels. *Nat. Commun.* **12**, 2082 (2021).
This work develops orthogonal photochemistry-assisted post-printing crosslinking for complex PEDOT:PSS-based 3D structures with high shape fidelity.
44. Shen, Z. et al. High-stretchability, ultralow-hysteresis conducting polymer hydrogel strain sensors for soft machines. *Adv. Mater.* **34**, 2203650 (2022).
This work constructs PEDOT:PSS-PVA hydrogels with a microphase-semiseparated network for highly sensitive low-hysteresis strain sensors at human–robot interfaces.
45. Zhou, T. et al. 3D printable high-performance conducting polymer hydrogel for all-hydrogel bioelectronic interfaces. *Nat. Mater.* **22**, 895–902 (2023).
This work reports monolithic bi-continuous PEDOT:PSS-PU hydrogels with high stretchability and stable electrical properties for fully printed all-hydrogel bioelectronic interfaces.
46. Yuk, H. et al. 3D printing of conducting polymers. *Nat. Commun.* **11**, 1604 (2020).
This work develops 3D-printable PEDOT:PSS inks via secondary dopants and enables high-resolution and high-aspect-ratio microstructures with overhanging features.
47. Kayser, L. V. & Lipomi, D. J. Stretchable conductive polymers and composites based on PEDOT and PEDOT:PSS. *Adv. Mater.* **31**, 1806133 (2019).
48. Truby, R. L. & Lewis, J. A. Printing soft matter in three dimensions. *Nature* **540**, 371–378 (2016).
49. Li, M., Pal, A., Aghakhani, A., Pena-Francesch, A. & Sitti, M. Soft actuators for real-world applications. *Nat. Rev. Mater.* **7**, 235–249 (2022).
50. Bertsch, P., Diba, M., Mooney, D. J. & Leeuwenburgh, S. C. G. Self-healing injectable hydrogels for tissue regeneration. *Chem. Rev.* **123**, 834–873 (2023).
51. Nezakati, T., Seifalian, A., Tan, A. & Seifalian, A. M. Conductive polymers: opportunities and challenges in biomedical applications. *Chem. Rev.* **118**, 6766–6843 (2018).
52. Yuk, H., Wu, J. J. & Zhao, X. H. Hydrogel interfaces for merging humans and machines. *Nat. Rev. Mater.* **7**, 935–952 (2022).
53. Zhu, T. et al. Recent advances in conductive hydrogels: classifications, properties, and applications. *Chem. Soc. Rev.* **52**, 473–509 (2023).
54. Wallin, T. J., Pikul, J. & Shepherd, R. F. 3D printing of soft robotic systems. *Nat. Rev. Mater.* **3**, 84–100 (2018).
55. Sachyani Keneth, E., Kamyshny, A., Totaro, M., Beccai, L. & Magdassi, S. 3D printing materials for soft robotics. *Adv. Mater.* **33**, 2003387 (2021).
56. Wang, D. et al. Soft actuators and robots enabled by additive manufacturing. *Annu. Rev. Control Rob. Auton. Syst.* https://doi.org/10.1146/annurev-control-061022-012035 (2023).
57. Zhou, J. A., Fukawa, T., Shirai, H. & Kimura, M. Anisotropic motion of electroactive papers coated with PEDOT/PSS. *Macromol. Mater. Eng.* **295**, 671–675 (2010).
58. Zheng, Y. et al. Coagulation bath-assisted 3D printing of PEDOT:PSS with high resolution and strong substrate adhesion for bioelectronic devices. *Adv. Mater. Technol.* **7**, 2101514 (2022).
This work reports a coagulation bath-assisted post-printing treatment to enable high resolution and strong substrate adhesion for bioelectronic devices.
59. Zhang, X. S., Yang, W. T., Zhang, H. N., Xie, M. Y. & Duan, X. X. PEDOT:PSS: from conductive polymers to sensors. *Nanotechnol. Precis. Eng.* **4**, 045004 (2021).
60. del Olmo, R., Mendes, T. C., Forsyth, M. & Casado, N. Mixed ionic and electronic conducting binders containing PEDOT:PSS and organic ionic plastic crystals toward carbon-free solid-state battery cathodes. *J. Mater. Chem. A* **10**, 19777–19786 (2022).
61. Zhang, J. et al. Ice-templated large-scale preparation of two-dimensional sheets of conjugated polymers: thickness-independent flexible supercapacitance. *ACS Nano* **15**, 8870–8882 (2021).
62. MacDiarmid, A. G. & Epstein, A. J. The concept of secondary doping as applied to polyaniline. *Synth. Met.* **65**, 103–116 (1994).
63. Tomaskovic-Crook, E. et al. Human neural tissues from neural stem cells using conductive biogel and printed polymer microelectrode arrays for 3D electrical stimulation. *Adv. Healthc. Mater.* **8**, 1900425 (2019).
64. Kee, S., Haque, M. A., Corzo, D., Alshareef, H. N. & Baran, D. Self-healing and stretchable 3D-printed organic thermoelectrics. *Adv. Funct. Mater.* **29**, 1905426 (2019).
65. Wang, W. et al. Inflight fiber printing toward array and 3D optoelectronic and sensing architectures. *Sci. Adv.* **6**, eaba0931 (2020).
This work reports overhanging PEDOT:PSS fibre arrays via continuous direct writing and enables moisture detection with precise temporal and spatial resolution.
66. Zhang, P., Aydemir, N., Alkaisi, M., Williams, D. E. & Travas-Sejdic, J. Direct writing and characterization of three-dimensional conducting polymer PEDOT arrays. *ACS Appl. Mater. Interfaces* **10**, 11888–11895 (2018).
67. Wang, Y. et al. A highly stretchable, transparent, and conductive polymer. *Sci. Adv.* **3**, 1602076 (2017).
68. Lu, B. et al. Pure PEDOT:PSS hydrogels. *Nat. Commun.* **10**, 1043 (2019).

69. Ouyang, J. et al. On the mechanism of conductivity enhancement in poly (3,4-ethylenedioxythiophene): poly(styrene sulfonate) film through solvent treatment. *Polymer* **45**, 8443–8450 (2004).
70. Yao, B. et al. Ultrahigh-conductivity polymer hydrogels with arbitrary structures. *Adv. Mater.* **29**, 1700974 (2017).
71. Kim, J., Zhang, G., Shi, M. & Suo, Z. Fracture, fatigue, and friction of polymers in which entanglements greatly outnumber cross-links. *Science* **374**, 212–216 (2021).
72. Zheng, Y., Zhang, S., Tok, J. B. & Bao, Z. Molecular design of stretchable polymer semiconductors: current progress and future directions. *J. Am. Chem. Soc.* **144**, 4699–4715 (2022).
73. Li, G. et al. Highly conducting and stretchable double-network hydrogel for soft bioelectronics. *Adv. Mater.* **34**, 2200261 (2022).
74. Zhao, Q. et al. Robust PEDOT:PSS-based hydrogel for highly efficient interfacial solar water purification. *Chem. Eng. J.* **442**, 136284 (2022).
75. Lei, Q., He, J. & Li, D. Electrohydrodynamic 3D printing of layer-specifically oriented, multiscale conductive scaffolds for cardiac tissue engineering. *Nanoscale* **11**, 15195–15205 (2019).
76. Chang, J., He, J., Lei, Q. & Li, D. Electrohydrodynamic printing of microscale PEDOT:PSS-PEO features with tunable conductive/thermal properties. *ACS Appl. Mater. Interfaces* **10**, 19116–19122 (2018).
77. Bao, P. et al. 3D printing PEDOT-CMC-based high areal capacity electrodes for Li-ion batteries. *Ionics* **27**, 2857–2865 (2021).
78. Taroni, P. J. et al. Toward stretchable self-powered sensors based on the thermoelectric response of PEDOT:PSS/polyurethane blends. *Adv. Funct. Mater.* **28**, 1704285 (2018).
79. Ahn, J. et al. Air-pressure-assisted pen-nib printing for 3D printed electronics. *Adv. Mater. Technol.* **7**, 2101172 (2021).
80. Yang, J. et al. 3D-printed highly stretchable conducting polymer electrodes for flexible supercapacitors. *J. Mater. Chem. A* **9**, 19649–19658 (2021).
This work prints PEDOT:PSS-based metastructures with negative Poisson's ratio for stretchable energy storage devices.
81. Alemu, D., Wei, H. Y., Ho, K. C. & Chu, C. W. Highly conductive PEDOT:PSS electrode by simple film treatment with methanol for ITO-free polymer solar cells. *Energy Environ. Sci.* **5**, 9662–9671 (2012).
82. Umrao, S. et al. MXene artificial muscles based on ionically cross-linked Ti(3)C(2)T(x) electrode for kinetic soft robotics. *Sci. Robot.* **4**, eaaw7797 (2019).
83. Chu, H. et al. Unipolar stroke, electroosmotic pump carbon nanotube yarn muscles. *Science* **371**, 494–498 (2021).
84. Pinilla, S., Coelho, J., Li, K., Liu, J. & Nicolosi, V. Two-dimensional material inks. *Nat. Rev. Mater.* **7**, 717–735 (2022).
85. Jiang, C. et al. Mammalian-brain-inspired neuromorphic motion-cognition nerve achieves cross-modal perceptual enhancement. *Nat. Commun.* **14**, 1344 (2023).
86. Liu, J. et al. Additive manufacturing of Ti_3C_2-MXene-functionalized conductive polymer hydrogels for electromagnetic-interference shielding. *Adv. Mater.* **34**, 2106253 (2022).
This work combines freeze–thawing and acid treatment to achieve both shape fidelity and high conductivity for printed PEDOT:PSS-MXene hydrogels.
87. Ghaffarkhah, A. et al. High-resolution extrusion printing of Ti_3C_2-based inks for wearable human motion monitoring and electromagnetic interference shielding. *Carbon* **191**, 277–289 (2022).
88. Xu, W. L., Du, Y. & Meng, Q. F. Fabrication of flexible thermoelectric composites by solution 3D printing technology. *Compos. Commun.* **28**, 100944 (2021).
89. Guo, J. et al. Loose pre-cross-linking mediating cellulose self-assembly for 3D printing strong and tough biomimetic scaffolds. *Biomacromolecules* **23**, 877–888 (2022).
90. Heo, D. N. et al. Development of 3D printable conductive hydrogel with crystallized PEDOT:PSS for neural tissue engineering. *Mater. Sci. Eng. C Mater. Biol. Appl.* **99**, 582–590 (2019).
91. Scordo, G. et al. A novel highly electrically conductive composite resin for stereolithography. *Mater. Today Commun.* **19**, 12–17 (2019).
92. Krainer, S., Smit, C. & Hirn, U. The effect of viscosity and surface tension on inkjet printed picoliter dots. *RSC Adv.* **9**, 31708–31719 (2019).
93. McKinley, G. H. & Renardy, M. Wolfgang von Ohnesorge. *Phys. Fluids* **23**, 127101 (2011).
94. Deegan, R. D. et al. Capillary flow as the cause of ring stains from dried liquid drops. *Nature* **389**, 827–829 (1997).
95. Du, Z. H., Zhou, H., Yu, X. H. & Han, Y. C. Controlling the polarity and viscosity of small molecule ink to suppress the contact line receding and coffee ring effect during inkjet printing. *Colloids Surf. A Physicochem. Eng. Asp.* **602**, 125111 (2020).
96. Doumenc, F. & Guerrier, B. Self-patterning induced by a solutal Marangoni effect in a receding drying meniscus. *Europhys. Lett.* **103**, 14001 (2013).
97. Deegan, R. D. et al. Contact line deposits in an evaporating drop. *Phys. Rev. E Stat. Phys. Plasmas Fluids Relat. Interdiscip. Topics* **62**, 756–765 (2000).
98. Saadi, M. et al. Direct ink writing: a 3D printing technology for diverse materials. *Adv. Mater.* **34**, 2108855 (2022).
This Review surveys commonly used rheological models for viscoelastic precursors in DIW.
99. Bao, Y. Recent trends in advanced photoinitiators for Vat photopolymerization 3D printing. *Macromol. Rapid Commun.* **43**, 2200202 (2022).
100. Wypych, G. *Handbook of UV Degradation and Stabilization* 2nd edn (ChemTec Publishing, 2015).
101. Zhu, H., Hu, X., Liu, B., Chen, Z. & Qu, S. 3D printing of conductive hydrogel-elastomer hybrids for stretchable electronics. *ACS Appl. Mater. Interfaces* **13**, 59243–59251 (2021).
This work reports soft hydrogel–elastomer hybrid devices with reliable adhesion interfaces and cross-scale structures via DLP.
102. Dadras-Toussi, O., Khorrami, M. & Abidian, M. R. Femtosecond laser 3D-printing of conductive microelectronics for potential biomedical applications. *Annu. Int. Conf. IEEE Eng. Med. Biol. Soc.* **2021**, 1197–1200 (2021).
103. Ahn, D., Stevens, L. M., Zhou, K. & Page, Z. A. Rapid high-resolution visible light 3D printing. *ACS Cent. Sci.* **6**, 1555–1563 (2020).
104. Lopez-Larrea, N. et al. Digital light 3D printing of PEDOT-based photopolymerizable inks for biosensing. *ACS Appl. Polym. Mater.* **4**, 6749–6759 (2022).
105. Mondschein, R. J., Kanitkar, A., Williams, C. B., Verbridge, S. S. & Long, T. E. Polymer structure–property requirements for stereolithographic 3D printing of soft tissue engineering scaffolds. *Biomaterials* **140**, 170–188 (2017).
106. Kee, S., Zhang, P. K. & Travas-Sejdic, J. Direct writing of 3D conjugated polymer micro/nanostructures for organic electronics and bioelectronics. *Polym. Chem.* **11**, 4530–4541 (2020).
107. Hu, J. & Yu, M. F. Meniscus-confined three-dimensional electrodeposition for direct writing of wire bonds. *Science* **329**, 313–316 (2010).
108. Kim, J. T. et al. Three-dimensional writing of highly stretchable organic nanowires. *ACS Macro Lett.* **1**, 375–379 (2012).
109. Chen, M., Xu, Z., Kim, J. H., Seol, S. K. & Kim, J. T. Meniscus-on-demand parallel 3D nanoprinting. *ACS Nano* **12**, 4172–4177 (2018).
This work reports an electrohydrodynamic dispensing approach for 3D parallel MGP with reliability and programmability.
110. Kim, J. T. et al. Three-dimensional writing of conducting polymer nanowire arrays by meniscus-guided polymerization. *Adv. Mater.* **23**, 1968–1970 (2011).
111. Li, M. Y., Nguyen, T. & Wang, J. Strip formation mechanisms and characteristics models in 3D printing of viscous polymer inks. *J. Manuf. Process.* **69**, 331–339 (2021).
112. Su, R., Park, S. H., Ouyang, X., Ahn, S. I. & McAlpine, M. C. 3D-printed flexible organic light-emitting diode displays. *Sci. Adv.* **8**, eabl8798 (2022).
This work reports a multimaterial printing platform, including extrusion, spray and mechanical reconfiguration, to explore fully printed flexible OLED displays for PEDOT:PSS.
113. Guo, Y. et al. PEDOT:PSS 'wires' printed on textile for wearable electronics. *ACS Appl. Mater. Interfaces* **8**, 26998–27005 (2016).
114. Roberts, T. et al. Flexible inkjet-printed multielectrode arrays for neuromuscular cartography. *Adv. Healthc. Mater.* **5**, 1462–1470 (2016).
115. Ngamna, O. et al. Inkjet printable polyaniline nanoformulations. *Langmuir* **23**, 8569–8574 (2007).
116. Monne, M. A., Lan, X., Zhang, C. B. & Chen, M. Y. H. Inkjet-printed flexible MEMS switches for phased-array antennas. *Int. J. Antennas Propag.* **2018**, 4517848 (2018).
117. Hinterbichler, H., Planchette, C. & Brenn, G. Ternary drop collisions. *Exp. Fluids* **56**, 190 (2015).
118. Teo, M. Y. et al. Direct patterning of highly conductive PEDOT:PSS/ionic liquid hydrogel via microreactive inkjet printing. *ACS Appl. Mater. Interfaces* **11**, 37069–37076 (2019).
119. Gao, X. X., Chen, H., Nie, Q. C. & Fang, H. S. Stability of line shapes in inkjet printing at low substrate speeds. *Phys. Fluids* **34**, 032002 (2022).
120. Shrestha, M., Lu, Z. & Lau, G. K. Transparent tunable acoustic absorber membrane using inkjet-printed PEDOT:PSS thin-film compliant electrodes. *ACS Appl. Mater. Interfaces* **10**, 39942–39951 (2018).
121. Maktabi, S. & Chiarot, P. R. Electrohydrodynamic printing of organic polymeric resistors on flat and uneven surfaces. *J. Appl. Phys.* **120**, 084903 (2016).
122. Basak, I. et al. Inkjet printing of PEDOT:PSS based conductive patterns for 3D forming applications. *Polymers* **12**, 2915 (2020).
123. Fan, J., Montemagno, C. & Gupta, M. 3D printed high transconductance organic electrochemical transistors on flexible substrates. *Org. Electron.* **73**, 122–129 (2019).
124. An, H. S. et al. High-resolution 3D printing of freeform, transparent displays in ambient air. *Adv. Sci.* **6**, 1901603 (2019).
This work reports a hybrid 3D printing platform to fabricate conformal optoelectronic architectures in ambient air.
125. Spencer, A. R. et al. Bioprinting of a cell-laden conductive hydrogel composite. *ACS Appl. Mater. Interfaces* **11**, 30518–30533 (2019).
126. Yuk, H. & Zhao, X. A new 3D printing strategy by harnessing deformation, instability, and fracture of viscoelastic inks. *Adv. Mater.* **30**, 1704028 (2018).
127. Zhu, J., Zhang, Q., Yang, T., Liu, Y. & Liu, R. 3D printing of multi-scalable structures via high penetration near-infrared photopolymerization. *Nat. Commun.* **11**, 3462 (2020).
128. Lee, Y. Y. et al. A strain-insensitive stretchable electronic conductor: PEDOT:PSS/acrylamide organogels. *Adv. Mater.* **28**, 1636–1643 (2016).
129. Yuk, H., Lu, B. & Zhao, X. Hydrogel bioelectronics. *Chem. Soc. Rev.* **48**, 1642–1667 (2019).
130. Yu, K. et al. Photosynthesis-assisted remodeling of three-dimensional printed structures. *Proc. Natl Acad. Sci. USA* **118**, e2016524118 (2021).
131. Xia, Y., Sun, K. & Ouyang, J. Solution-processed metallic conducting polymer films as transparent electrode of optoelectronic devices. *Adv. Mater.* **24**, 2436–2440 (2012).
132. Saxena, N. et al. Ionic liquids as post-treatment agents for simultaneous improvement of Seebeck coefficient and electrical conductivity in PEDOT:PSS films. *ACS Appl. Mater. Interfaces* **11**, 8060–8071 (2019).
133. Bertana, V. et al. Rapid prototyping of 3D organic electrochemical transistors by composite photocurable resin. *Sci. Rep.* **10**, 13335 (2020).

134. Lee, S. H., Park, W. S., Cho, H. S., Zhang, W. & Leu, M. C. A neural network approach to the modelling and analysis of stereolithography processes. *Proc. Inst. Mech. Eng. B J. Eng. Manuf.* **215**, 1719–1733 (2001).
135. Scordo, G. et al. Effect of volatile organic compounds adsorption on 3D-printed PEGDA:PEDOT for long-term monitoring devices. *Nanomaterials* **11**, 94 (2021).
136. Xing, J. F., Zheng, M. L. & Duan, X. M. Two-photon polymerization microfabrication of hydrogels: an advanced 3D printing technology for tissue engineering and drug delivery. *Chem. Soc. Rev.* **44**, 5031–5039 (2015).
137. Patil, A. O., Heeger, A. J. & Wudl, F. Optical properties of conducting polymers. *Chem. Rev.* **88**, 183–200 (1988).
138. Kurselis, K., Kiyan, R., Bagratashvili, V. N., Popov, V. K. & Chichkov, B. N. 3D fabrication of all-polymer conductive microstructures by two photon polymerization. *Opt. Express* **21**, 31029–31035 (2013).
139. Tao, Y. et al. Nanostructured electrically conductive hydrogels obtained via ultrafast laser processing and self-assembly. *Nanoscale* **11**, 9176–9184 (2019).
140. Geng, Q., Wang, D., Chen, P. & Chen, S. C. Ultrafast multi-focus 3-D nano-fabrication based on two-photon polymerization. *Nat. Commun.* **10**, 2179 (2019).
141. Sun, C., Fang, N., Wu, D. M. & Zhang, X. Projection micro-stereolithography using digital micro-mirror dynamic mask. *Sens. Actuator A Phys.* **121**, 113–120 (2005).
142. Kim, S., Handler, J. J., Cho, Y. T., Barbastathis, G. & Fang, N. X. Scalable 3D printing of aperiodic cellular structures by rotational stacking of integral image formation. *Sci. Adv.* **7**, eabh1200 (2021).
143. Aggas, J. R., Abasi, S., Phipps, J. F., Podstawczyk, D. A. & Guiseppi-Elie, A. Microfabricated and 3-D printed electroconductive hydrogels of PEDOT:PSS and their application in bioelectronics. *Biosens. Bioelectron.* **168**, 112568 (2020).
144. Sunwoo, S. H., Ha, K. H., Lee, S., Lu, N. & Kim, D. H. Wearable and implantable soft bioelectronics: device designs and material strategies. *Annu. Rev. Chem. Biomol. Eng.* **12**, 359–391 (2021).
145. Zhao, Z., Spyropoulos, G. D., Cea, C., Gelinas, J. N. & Khodagholy, D. Ionic communication for implantable bioelectronics. *Sci. Adv.* **8**, eabm7851 (2022).
146. Chaudhuri, O., Cooper-White, J., Janmey, P. A., Mooney, D. J. & Shenoy, V. B. Effects of extracellular matrix viscoelasticity on cellular behaviour. *Nature* **584**, 535–546 (2020).
147. Lou, J. & Mooney, D. J. Chemical strategies to engineer hydrogels for cell culture. *Nat. Rev. Chem.* **6**, 726–744 (2022).
148. Vernerey, F. J., Lalitha Sridhar, S., Muralidharan, A. & Bryant, S. J. Mechanics of 3D cell–hydrogel interactions: experiments, models, and mechanisms. *Chem. Rev.* **121**, 11085–11148 (2021).
149. Park, S. E. et al. Geometric engineering of organoid culture for enhanced organogenesis in a dish. *Nat. Methods* **19**, 1449–1460 (2022).
150. Rastin, H. et al. 3D printing of cell-laden electroconductive bioinks for tissue engineering applications. *J. Mater. Chem. B* **8**, 5862–5876 (2020).
151. Cogan, S. F. Neural stimulation and recording electrodes. *Annu. Rev. Biomed. Eng.* **10**, 275–309 (2008).
152. Yao, B. et al. Ultrastrong, highly conductive and capacitive hydrogel electrode for electron-ion transduction. *Matter* **5**, 4407–4424 (2022).
153. Nolan, J. K., Nguyen, T. N. H., Le, K. V. H., DeLong, L. E. & Lee, H. Simple fabrication of flexible biosensor arrays using direct writing for multianalyte measurement from human astrocytes. *SLAS Technol.* **25**, 33–46 (2020).
154. Tan, P. et al. Solution-processable, soft, self-adhesive, and conductive polymer composites for soft electronics. *Nat. Commun.* **13**, 358 (2022).
155. Liu, H. et al. 3D printed flexible strain sensors: from printing to devices and signals. *Adv. Mater.* **33**, 2004782 (2021).
156. Liu, H. et al. Harnessing the wide-range strain sensitivity of bilayered PEDOT:PSS films for wearable health monitoring. *Matter* **4**, 2886–2901 (2021).
157. Olowo, O. O. et al. *2022 IEEE International Conference on Flexible and Printable Sensors and Systems* (*FLEPS*), Vienna, Austria, 1–4 (IEEE, 2022).
158. Kim, J., Campbell, A. S., de Avila, B. E. & Wang, J. Wearable biosensors for healthcare monitoring. *Nat. Biotechnol.* **37**, 389–406 (2019).
159. Sempionatto, J. R., Lasalde-Ramirez, J. A., Mahato, K., Wang, J. & Gao, W. Wearable chemical sensors for biomarker discovery in the omics era. *Nat. Rev. Chem.* **6**, 899–915 (2022).
160. Wang, Y. et al. Skin bioelectronics towards long-term, continuous health monitoring. *Chem. Soc. Rev.* **51**, 3759–3793 (2022).
161. Rivnay, J. et al. Organic electrochemical transistors. *Nat. Rev. Mater.* **3**, 17086 (2018).
162. Majak, D., Fan, J. X. & Gupta, M. Fully 3D printed OECT based logic gate for detection of cation type and concentration. *Sens. Actuators B Chem.* **286**, 111–118 (2019).
163. Keene, S. T. et al. Enhancement-mode PEDOT:PSS organic electrochemical transistors using molecular de-doping. *Adv. Mater.* **32**, 2000270 (2020).
164. Su, X. et al. A highly conducting polymer for self-healable, printable, and stretchable organic electrochemical transistor arrays and near hysteresis-free soft tactile sensors. *Adv. Mater.* **34**, 2200682 (2022).
165. Maksimkin, A. V., Dayyoub, T., Telyshev, D. V. & Gerasimenko, A. Y. Electroactive polymer-based composites for artificial muscle-like actuators: a review. *Nanomaterials* **12**, 2272–2292 (2022).
166. Chortos, A., Hajiesmaili, E., Morales, J., Clarke, D. R. & Lewis, J. A. 3D printing of interdigitated dielectric elastomer actuators. *Adv. Funct. Mater.* **30**, 1907375 (2020).
167. Christianson, C., Goldberg, N. N., Deheyn, D. D., Cai, S. & Tolley, M. T. Translucent soft robots driven by frameless fluid electrode dielectric elastomer actuators. *Sci. Robot.* **3**, eaat1893 (2018).
168. Shrestha, M., Asundi, A. & Lau, G. K. Smart window based on electric unfolding of microwrinkled TiO_2 nanometric films. *ACS Photonics* **5**, 3255–3262 (2018).
169. Chen, L., Busfield, J. J. C. & Carpi, F. Electrically tunable directional light scattering from soft thin membranes. *Opt. Express* **28**, 20669–20685 (2020).
170. Wang, Y., Li, P., Gupta, U., Ouyang, J. & Zhu, J. Tunable soft lens of large focal length change. *Soft Robot.* **9**, 705–712 (2022).
171. Li, P. C. et al. Transparent soft robots for effective camouflage. *Adv. Funct. Mater.* **29**, 1901908 (2019).
172. Jager, E. W., Smela, E. & Inganas, O. Microfabricating conjugated polymer actuators. *Science* **290**, 1540–1545 (2000).
173. Feng, C., Hemantha Rajapaksha, C. P. & Jákli, A. Ionic elastomers for electric actuators and sensors. *Engineering* **7**, 581–602 (2021).
174. Park, M., Yoo, S., Bae, Y., Kim, S. & Jeon, M. Enhanced stability and driving performance of GO(-)Ag-NW-based ionic electroactive polymer actuators with Triton X-100-PEDOT:PSS nanofibrils. *Polymers* **11**, 906–914 (2019).
175. Park, M., Kim, J., Song, H., Kim, S. & Jeon, M. Fast and stable ionic electroactive polymer actuators with PEDOT:PSS/(graphene(-)Ag-nanowires) nanocomposite electrodes. *Sensors* **18**, 3126–3139 (2018).
176. Põldsalu, I. et al. Thin ink-jet printed trilayer actuators composed of PEDOT:PSS on interpenetrating polymer networks. *Sens. Actuators B Chem.* **258**, 1072–1079 (2018).
177. Simaite, A., Mesnilgrente, F., Tondu, B., Soueres, P. & Bergaud, C. Towards inkjet printable conducting polymer artificial muscles. *Sens. Actuators B Chem.* **229**, 425–433 (2016).
178. Nakshatharan, S. S., Martinez, J. G., Punning, A., Aabloo, A. & Jager, E. W. H. Soft parallel manipulator fabricated by additive manufacturing. *Sens. Actuators B Chem.* **305**, 127355 (2020).
179. Tian, Y., Li, Y. T., Tian, H., Yang, Y. & Ren, T. L. Recent progress of soft electrothermal actuators. *Soft Robot.* **8**, 241–250 (2021).
180. Zhan, Z. et al. 3D printed ultra-fast photothermal responsive shape memory hydrogel for microrobots. *Int. J. Extrem. Manuf.* https://doi.org/10.1088/2631-7990/ac376b (2021).
181. Todd, S. T. & Huikai, X. An electrothermomechanical lumped element model of an electrothermal bimorph actuator. *J. Microelectromech. Syst.* **17**, 213–225 (2008).
182. Shakoor, A., Gao, W., Zhao, L., Jiang, Z. & Sun, D. Advanced tools and methods for single-cell surgery. *Microsyst. Nanoeng.* **8**, 47 (2022).
183. Yao, Z.-F., Wang, J.-Y. & Pei, J. Controlling morphology and microstructure of conjugated polymers via solution-state aggregation. *Prog. Polym. Sci.* **136**, 101626 (2023).
184. Liu, G. et al. Additive manufacturing of structural materials. *Mater. Sci. Eng. R. Rep.* **145**, 100596 (2021).
185. Kollamaram, G. et al. Low temperature fused deposition modeling (FDM) 3D printing of thermolabile drugs. *Int. J. Pharm.* **545**, 144–152 (2018).
186. Huang, J., Ware, H. O. T., Hai, R., Shao, G. & Sun, C. Conformal geometry and multimaterial additive manufacturing through freeform transformation of building layers. *Adv. Mater.* **33**, 2005672 (2021).
187. Zhang, K. et al. Aerial additive manufacturing with multiple autonomous robots. *Nature* **609**, 709–717 (2022).
188. Hua, M. et al. Strong tough hydrogels via the synergy of freeze-casting and salting out. *Nature* **590**, 594–599 (2021).
189. Chen, J. et al. 3D-printed anisotropic polymer materials for functional applications. *Adv. Mater.* **34**, 2102877 (2022).
190. Weeks, R. D., Truby, R. L., Uzel, S. G. M. & Lewis, J. A. Embedded 3D printing of multimaterial polymer lattices via graph-based print path planning. *Adv. Mater.* **35**, e2206958 (2022).
191. Wijsboom, Y. H. et al. Controlling rigidity and planarity in conjugated polymers: poly(3,4-ethylenedithioselenophene). *Angew. Chem.* **121**, 5551–5555 (2009).
192. Xu, Y. et al. Molecular engineered conjugated polymer with high thermal conductivity. *Sci. Adv.* **4**, eaar3031 (2018).
193. Cui, C. & Liu, W. Recent advances in wet adhesives: adhesion mechanism, design principle and applications. *Prog. Polym. Sci.* **116**, 101388 (2021).
194. Ji, S. & Chen, X. Enhancing the interfacial binding strength between modular stretchable electronic components. *Natl Sci. Rev.* **10**, nwac172 (2023).
195. Inoue, A., Yuk, H., Lu, B. & Zhao, X. Strong adhesion of wet conducting polymers on diverse substrates. *Sci. Adv.* **6**, eaay5394 (2020).
196. Rao, Z. Y. et al. Curvy, shape-adaptive imagers based on printed optoelectronic pixels with a kirigami design. *Nat. Electron.* **4**, 513–521 (2021).
197. Lv, J., Thangavel, G. & Lee, P. S. Reliability of printed stretchable electronics based on nano/micro materials for practical applications. *Nanoscale* **15**, 434–449 (2023).
198. Zuo, R., Zhou, Z., Ying, B. & Liu, X. in *2021 IEEE International Conference on Robotics and Automation* (*ICRA*) 12164–12169 (IEEE, 2021).
199. Wang, K. et al. 3D printing of viscoelastic suspensions via digital light synthesis for tough nanoparticle–elastomer composites. *Adv. Mater.* **32**, 2001646 (2020).
200. Wehner, M. et al. An integrated design and fabrication strategy for entirely soft, autonomous robots. *Nature* **536**, 451–455 (2016).
201. Becker, K. et al. Active entanglement enables stochastic, topological grasping. *Proc. Natl Acad. Sci. USA* **119**, 2209819119 (2022).
202. Shen, Z., Zhu, X., Majidi, C. & Gu, G. Cutaneous ionogel mechanoreceptors for soft machines, physiological sensing, and amputee prostheses. *Adv. Mater.* **33**, 2102069 (2021).

203. Dobashi, Y. et al. Piezoionic mechanoreceptors: force-induced current generation in hydrogels. *Science* **376**, 502–507 (2022).
204. Allard, C. An all-polymer display for on-skin electronics. *Nat. Rev. Mater.* **7**, 335–335 (2022).
205. Li, K. et al. 4D printing of MXene hydrogels for high-efficiency pseudocapacitive energy storage. *Nat. Commun.* **13**, 6884 (2022).
206. Yang, C. Y. et al. A high-conductivity n-type polymeric ink for printed electronics. *Nat. Commun.* **12**, 2354 (2021).
207. Ouyang, X. et al. 3D printed skin-interfaced UV-visible hybrid photodetectors. *Adv. Sci.* **9**, 2201275 (2022).
208. Song, S., Fallegger, F., Trouillet, A., Kim, K. & Lacour, S. P. Deployment of an electrocorticography system with a soft robotic actuator. *Sci. Robot.* **8**, eadd1002 (2023).
209. Zhu, J. et al. Intelligent soft surgical robots for next-generation minimally invasive surgery. *Adv. Intell. Syst.* **3**, 2100011 (2021).
210. Bradley, C., Nydam, A. S., Dux, P. E. & Mattingley, J. B. State-dependent effects of neural stimulation on brain function and cognition. *Nat. Rev. Neurosci.* **23**, 459–475 (2022).
211. Chao, Y. et al. One-pot hydrothermal synthesis of solution-processable MoS_2/PEDOT:PSS composites for high-performance supercapacitors. *ACS Appl. Mater. Interfaces* **13**, 7285–7296 (2021).
212. Groenendaal, B. L., Jonas, F., Freitag, D., Pielartzik, H. & Reynolds, J. R. Poly(3,4-ethylenedioxythiophene) and its derivatives: past, present, and future. *Adv. Mater.* **12**, 481–494 (2000).
213. Yang, Y., Deng, H. & Fu, Q. Recent progress on PEDOT:PSS based polymer blends and composites for flexible electronics and thermoelectric devices. *Mater. Chem. Front.* **4**, 3130–3152 (2020).
214. Elschner, A., Kirchmeyer, S., Lovenich, W., Merker, U. & Reuter, K. *PEDOT: Principles and Applications of an Intrinsically Conductive Polymer* 1st edn, 113–158 (CRC Press, 2010).

Acknowledgements
The authors thank D. Wang for constructive suggestions and essay polishing on printing techniques, Z. Shen for the insightful discussion on perspective applications for soft machines at human–robot interfaces and Q. Zhao for his keen percipience on design principles of printable inks. This study was supported in part by the National Natural Science Foundation of China (Grant Nos 52025057, 51963011 and T2293725.), the Science and Technology Commission of Shanghai Municipality (Grant No. 20550712100) and the Innovative Research Team of High-Level Local Universities in Shanghai (SHSMU-ZDCX20210901).

Author contributions
J.L. and J.C. contributed equally to this paper. All authors contributed to the planning, discussion and writing of the manuscript.

Competing interests
The authors declare no competing interests.

Additional information
Peer review information *Nature Reviews Materials* thanks Chuan-Fei Guo, Shaoxing Qu and Wentao Xu for their contribution to the peer review of this work.

Publisher's note Springer Nature remains neutral with regard to jurisdictional claims in published maps and institutional affiliations.